The Identification of Differentially Expressed Genes in Nasal Swabs from Chronic Wasting Disease-Infected White-tailed Deer

A THESIS SUBMITTED TO
THE FACULTY OF THE GRADUATE SCHOOL
OF THE UNIVERSITY OF MINNESOTA
BY

Peizhi Zou

IN PARTIAL FULFILLMENT OF THE REQUIREMENTS
FOR THE DEGREE OF
MASTER OF SCIENCE

2023

Acknowledgments

I would like to express my gratitude to everyone who helped me to complete this project. Dr. Justin Greenlee and Dr. Eric Cassmann kindly collected and provided me with these precious nasal swab samples from white-tailed deer. Great thanks to Dr. Elyse Froehling, all experts and resources from the University of Minnesota Genomics Center (UMGC), who performed the next-generation total RNA sequencing and RNA quantification. This work was completed and supported by resources provided by UMGC. I acknowledge the staff and resources at the Minnesota Supercomputing Institute (MSI) at the University of Minnesota for contributing to the research results reported within this thesis. Dr. Natalia Calixto Mancipe from MSI and Dr. Juan E Abrahante Lloréns from the University of Minnesota Informatics Institute (UMII) helped me to analyze the sequencing data from UMGC; it is impossible for me to finish this project without their support and help. I also deeply appreciate the help from Ms. Madeline Ellefson, who performed PCR experiments with me. Many thanks to Dr. Emily Sevcik, Dr. Mary Pampusch, and Dr. Pongthorn Pumtang-on; they provide invaluable support in drafting, graphing, and experiment design. Thanks to Negin Goodarzi, who trained me and completed the RNA extraction with me. I appreciate the funding support from the State of MN LCCMR grant, the State of MN MAES RARF grant, and the UMN small seed grant for this project. Last but not least, I want to thank my supervisor, Dr. Pamela Skinner, who provided help and support from all perspectives and guided me to fulfill this study.

Abstract

Chronic wasting disease (CWD) is a transmissible spongiform encephalopathy (TSE) or prion disease, which is spreading in cervid populations, including mule deer (*Odocoileus hemionus*), white-tailed deer (*Odocoileus virginianus*), and Rocky Mountain elk (*Cervus elaphus nelsoni*). The pathogen of CWD is the abnormally misfolded prion protein (PrPsc) which is converted from normal function cellular prion protein (PrPc). PrPc is coded by the PRNP gene which is highly expressed in the central nervous system (CNS) and also expressed in the peripheral nervous system. The specific biological function of PrPc in CNS still remains unclear and the pathogenesis of the PrPsc also needs a better understanding. CWD is spreading fast in many places around the world, and CWD is fatal to all infected animals with no treatment or vaccine for it. Our final goal of this research is to develop a diagnosis and treatment approach for CWD. I hypothesize that there are differentially expressed genes (DEGs) caused by CWD in the nasal brush samples, and the identified DEGs could be used for CWD diagnosis.
This study used next-generation total RNA sequencing to identify potential biomarkers in nasal swab samples from CWD white-tailed deer and increase understanding of CWD pathogenesis. We annotated and filtered genes from the reference genome and identified DEGs consistently altered in late-stage post-infection samples. Additionally, we performed Gene Set Enrichment Analysis for these identified genes at each time point, and we found cell proliferation pathways were suppressed, and immune response pathways were activated post-CWD infection. These biomarkers and pathways could provide some new insights into CWD diagnosis and CWD treatment for future research.

Table of Contents

List of Abbreviations

DEGs: differentially expressed genes

NS: nasal swab

CWD: Chronic wasting disease

TSE: transmissible spongiform encephalopathy

PrPc: cellular prion protein

PrPsc: misfolded prion protein

CJD: Creutzfeldt-Jakob disease

sCJD: sporadic Creutzfeldt-Jakob disease

gCJD: genetic Creutzfeldt-Jakob disease

iCJD: iatrogenic Creutzfeldt-Jakob disease

vCJD: variant Creutzfeldt-Jakob disease

FFI: fatal familial insomnia

GSS: Gerstmann–Straüssler–Scheinker disease

BSE: bovine spongiform encephalopathy

TME: transmissible mink encephalopathy

HY: the hyper PrPsc

DY: the drowsy PrPsc

CNS: central nervous system

GPI: glycosylphosphatidylinositol

DC: dendritic cells

FDC: follicular dendritic cells

SLO: secondary lymphoid organs

IHC: immunohistochemistry

ELISA: enzyme-linked immunoassays

WB: western blot

PMCA: protein misfolding cyclic amplification

RT-QuIC: real-time quaking-induced conversion

OS: olfactory system

MPI: month post-infection

PCA: principal component analysis

RIN: RNA integrity number

NGS: Next-generation sequencing

GSEA: gene set enrichment analysis

GO: gene ontology

MSigDB: Molecular Signatures Database

BP: biological process

MF: molecular function

CC: cellular component

KEGG: Kyoto Encyclopedia of Genes and Genomes database

ES: enrichment score

NES: normalized enrichment score

FDR: false discovery rate

ER stress: endoplasmic reticulum stress

OSE: olfactory sensory epithelium

ORN: olfactory receptor neurons

List of Tables

List of Figures

Chapter One

Introduction to Chronic Wasting Disease

Abstract

Prion diseases or transmissible spongiform encephalopathies (TSEs) are a group of contagious, fatal, incurable neurodegenerative diseases caused by the misfolded prion protein (PrPsc, which has a β-sheet-rich structure), which was converted from normal prion protein (PrPc, which has an α-helical-rich structure) in neuronal tissue. Prion diseases affect both animals and humans which brings severe public concerns in the food and health industry. Currently, there is no treatment for any of the prion diseases and all infected individuals generally die within observed clinical signs or symptoms within several years. Prion diseases typical clinical symptoms are rapidly developing dementia, behavior changes, difficulty walking and changes in gait, hallucinations, and muscle stiffness. Prion-infected brain histological analysis usually shows spongiform degeneration, neuronal loss, and amyloid plaque accumulation with astrocytosis.

Brief Prion Diseases History and Introduction

Human prion diseases

Creutzfeldt-Jakob disease (CJD)

Creutzfeldt-Jakob disease (CJD) is the most common form of human prion disease or transmissible spongiform encephalopathies (TSE)[1,2]. Currently, four types of CJD have been identified based on their different etiology: sporadic (sCJD), familial or genetic (gCJD); iatrogenic (iCJD), and variant CJD (vCJD).[3,4] Hans Gerhardt Creutzfeldt and Alfons Maria Jakob were considered the first two people to describe this disease`s syndrome in 1920 and the term “CJD” case was first introduced by Spielmeyer in 1922 to describe the neurodegenerative conditions[5–7]. The major clinical features of CJD include fatigue, insomnia, depression, weight loss, headaches, and malaise. Variant CJD (vCJD) is caused by the consumption of BSE-contaminated food[8]. Sporadic CJD is thought to result from the abnormal conversion of normal cellular prion protein PrPc into its misfolded PrPsc and was reported at a rate of 1-2 cases per million worldwide[9,10]. Familial or genetic CJD accounts for approximately 10-15% of CJD and is caused by inherited mutations in the PRNP gene[11]. Iatrogenic CJD is extremely rare and arises due to medical or surgical procedures, accounting for only 1% of CJD cases[12].

Kuru

Kuru was first discovered in Papua New Guinea among cannibalistic tribes around 1900 and was recognized as a disease around 1940-1950[13]. Kuru is caused by prions in contaminated human brain tissue, resulting from a funeral ritual practiced by the Fore people of New Guinea, in which they consumed the brains of deceased individuals.

After the Fore people stopped this ritual in the early 1960s, the transmission of Kuru gradually declined. The last reported Kuru case was in 2005 or 2009, and the disease is now considered extinct[14].

Fatal Familial Insomnia (FFI)

Fatal familial insomnia (FFI) is an inherited prion disease caused by a mutation at codon 178 of the PRNP prion gene[15]. It is characterized by the inability to sleep and dysautonomia. FFI was first described in 1986[16].

Gerstmann–Straüssler–Scheinker disease (GSS)

Gerstmann–Straüssler–Scheinker disease (GSS) is an extremely rare, slowly progressive, hereditary neurodegenerative disease. It was described by Dimitz in 1913 and Gerstmann in 1928[17]. GSS is caused by an autosomal dominant disorder[18], and specific mutations at codons 102, 105, 117, 145, 198, and 217 of the open reading frame of the prion protein gene are associated with GSS disease. GSS typically occurs at an earlier age around 40, and the average duration of illness is five years.

Animal prion diseases

Bovine spongiform encephalopathy (BSE)

Bovine spongiform encephalopathy (BSE), also known as “mad cow disease,” is a TSE affecting cattle. It was first recognized in the United Kingdom in 1986. The BES epidemic was likely caused by the recycling of infected bovine tissues and the feeding of ruminant-derived protein to other ruminants prior to the recognition of BSE.[19–21]

Scrapie

Scrapie is a naturally occurring prion disease affecting sheep and goats and has been known in Europe for over 250 years[22]. Clinical signs of scrapie include behavior changes and increased aggressiveness[23]. The name “scrapie” is derived from one clinical sign that the infected animal will compulsively scrape off their fleeces due to the itchiness caused by scrapie infection[24].

Transmissible mink encephalopathy (TME)

Transmissible mink encephalopathy (TME) is a rare and progressive TSE that affects ranch-raised mink (*Mustela*) [25]. TME has two strains of PrPsc that can be converted from the same PrPc: the hyper (HY) and the drowsy (DY)[26,27]. These two strains exhibit stable variations due to conformational differences, the HY PrPsc showed higher proteinase K resistance compared to the DY PrPsc[26,28].

Chronic wasting disease (CWD)

In 1967, the first chronic wasting disease case was reported among captive mule deer (*Odocoileus hemionus*) as a clinical syndrome with unknown etiology in a wildlife research facility in Colorado and another wildlife research facility in Wyoming[29,30]. In 1978, CWD was first diagnosed as a spongiform encephalopathy. In 1981, the CWD was found in a free-ranging elk in Colorado. CWD was also found in free-ranging mule deer and white-tailed deer (*Odocoileus virginianus*) in these two states in 1986 and 1990. Chronic wasting disease has been spreading fast in many states and nations around the world. Since 2000, at least 29 states in the USA have reported the occurrence of CWD in free-ranging deer and localized infection rates of more than 25 percent[31].

Prion Diseases Pathogenesis

Prion disease pathogenesis is attributed to the abnormal misfolding of the prion protein (PrPsc) from its normal cellular form (PrPc). The PrPc is expressed widely on the cell membrane via its glycosylphosphatidylinositol (GPI) anchor in both neural and nonneural tissues, with expression at the highest level in neurons in the central nervous system (CNS)[32,33]. Though the pathological relevance of PrP is now established, the specific functions of PrPc still remain unclear. Three hypothesized functions have been indicated: 1) PrPc is a metal ion-binding protein as it binds to copper and zinc with low micromolar affinity[34,35]; 2) PrPc may play a major role in cell survival and differentiation [36,37]; 3) PrPc acts as a role in the recycling of the vesicles or a more direct role in synaptic activity[38–40]. A well-characterized property of the physiological PrPc is its native structure, which is composed of a disordered N-terminal flexible tail (residues 23–124) and a structured C-terminal region (125–230) composed of three α-helix structures and a short antiparallel β-sheet[41].

PrPc is coded in the PRNP gene which is highly conserved among many species[42,43]. In a scrapie study, PRNP gene knock-out mice showed resistance to scrapie and indicated PrPc is the prerequisite of prion infection and development[44,45]. Mutations in the PRNP gene influence susceptibility to prion diseases[46,47]. In a scrapie-sheep study, a set of allele variants in positions 136, 154, and 171 of the PrP sequence are recognized to affect scrapie susceptibility. Genotype A136-R154-R171 was scrapie resistant, whereas V136-R154-Q171 showed high scrapie susceptibility. A136-R154-Q171 and A136-H154-Q171 variants are medium and low scrapie susceptibility.

PRNP is a single-copy gene that spans 16 kb, is comprised of 2 exons[48], and encodes a 253 amino acid protein in the larger second exon[49,50]. The N-terminal region of the protein contains an octapeptide copper-binding repeat domain[51]. Various mutations

within the Cu2+-binding region might be involved in prion pathogenesis[52]. The C-terminal domain of PrP is N-glycosylated and GPI-anchored to the cell's outer-membrane[53,54].

The structure of PrPsc and PrPc are shown in **Figure 1**. The PrPsc serves as a self-template and catalyst for the conversion (**Figure 2**) of the normal PrPc into its misfolded form PrPsc and then aggregates into prion amyloid[55]. The conversion is not yet fully understood but is considered to be spontaneous and triggered by PrPsc[56–58]. PrPsc is partially resistant to proteinase digestion[59,60].

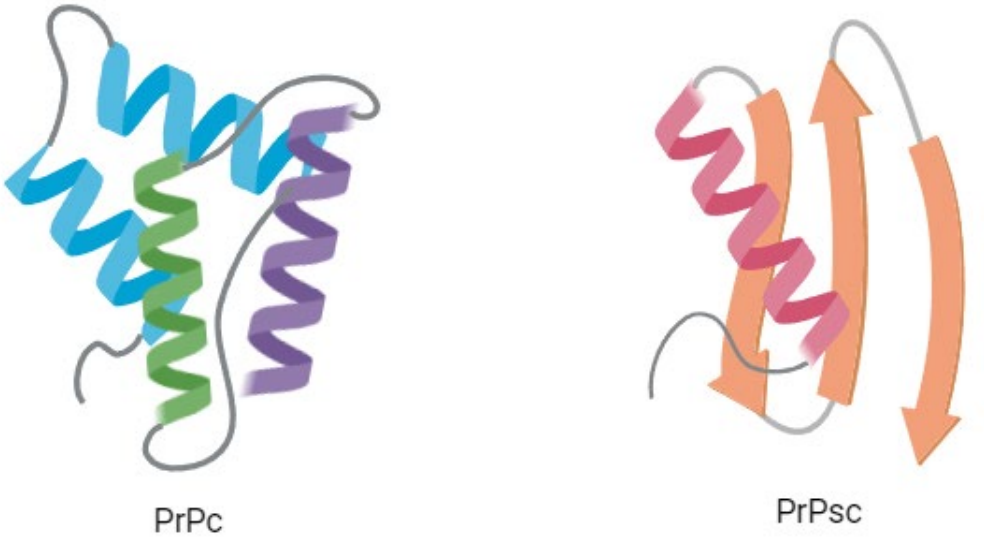

Figure 1. Page 6. Illustration of prion protein structures. The PrPc (left) is rich in α-helical structures (coils). Conformational change into PrPsc (right) results in replacement by amyloidogenic β-pleated strands (arrows). Made by Biorender.

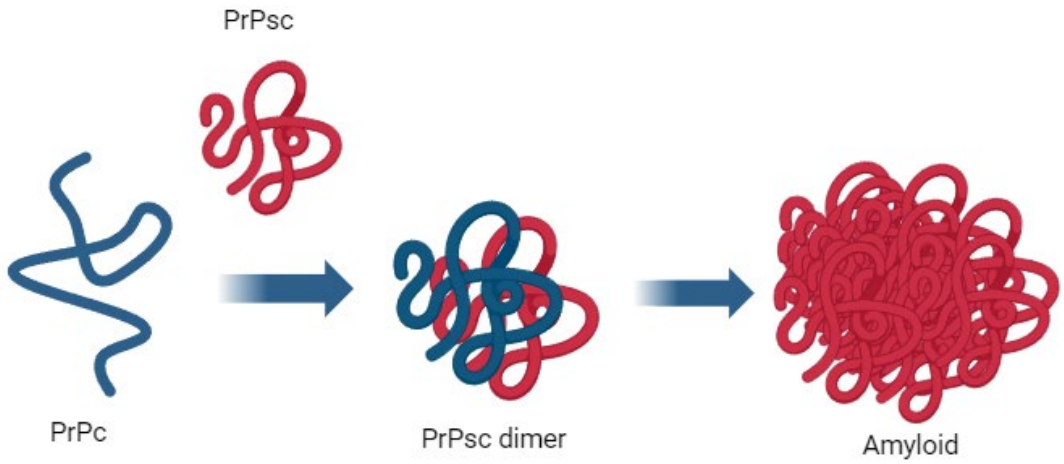

Figure 2. Page 7. Illustration of PrPsc self-template conversion. PrPsc initiates and catalyzes this self-template conversion, and converts PrPc into a PrPsc dimer. Prion amyloid will form due to PrPsc accumulation and aggregation. Made by Biorender.

PrPsc accumulates in lymphoid tissue and the CNS, leading to the spongiform changes observed in late-stage brain tissues of prion-infected individuals. The influence of PrPsc on neuron tissue and its role in cell apoptosis and autophagy are still areas of debate in the scientific community[61].

Prion Protein Transmission

The potential transmission routes of animal prion diseases are shown in **Figure 3**. The transmitted route might depend on factors like the host development stage and cultivation conditions [62–64]. Prion diseases such as scrapie in sheep, CWD in cervid species, and BSE in cattle are considered to be infected via the oral route [20,65–67].

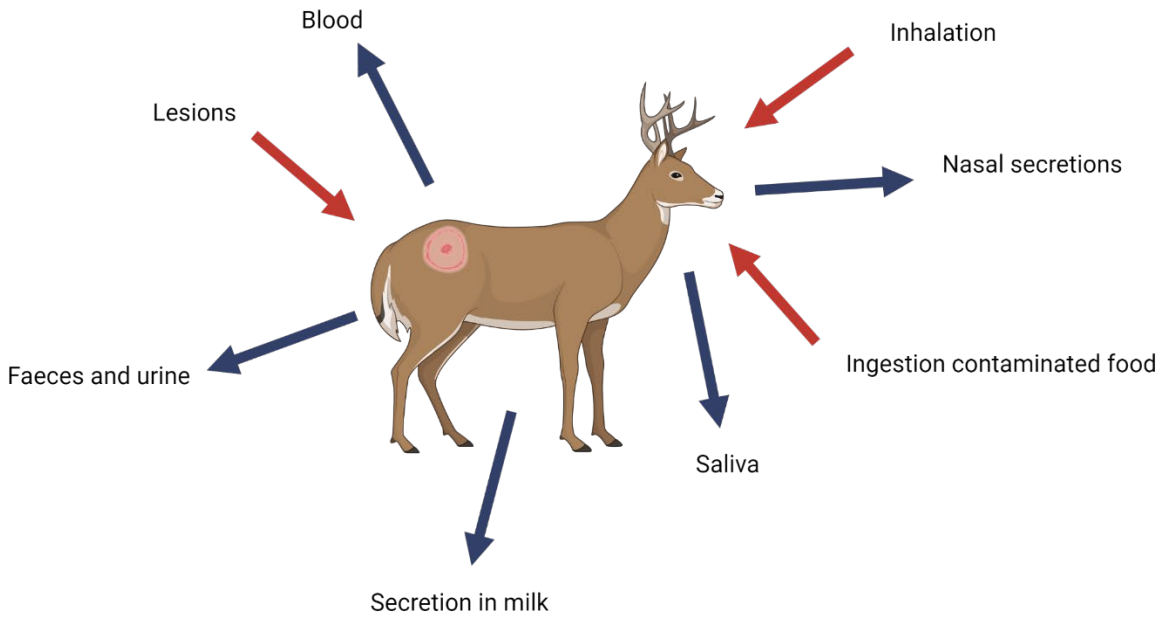

Figure 3. Page 8. Potential routes of prion exposure and dissemination. Red arrows: routes of prion exposure; blue arrows: routes of prion secretion. Made by Biorender.

The spreading of orally infected prion disease is shown in **Figure 4**, the prions must first cross the gut epithelium via M cells and be delivered by conventional dendritic cells (DC)[68], then PrPsc first accumulated in the secondary lymphoid organs[69]. Mouse studies have shown that prions accumulate upon the surface of follicular dendritic cells (FDC) within the B cell follicles of secondary lymphoid organs (SLO) within days of peripheral infection[70,71]. When the prions on the FDC surface are amplified to above the required threshold to achieve neuroinvasion, prions subsequently infect local sympathetic and parasympathetic neurons in the SLO and spread along them to the CNS[70,72,73]. However, the mechanism by which the prions are propagated between FDC and the peripheral nervous system is undetermined[74].

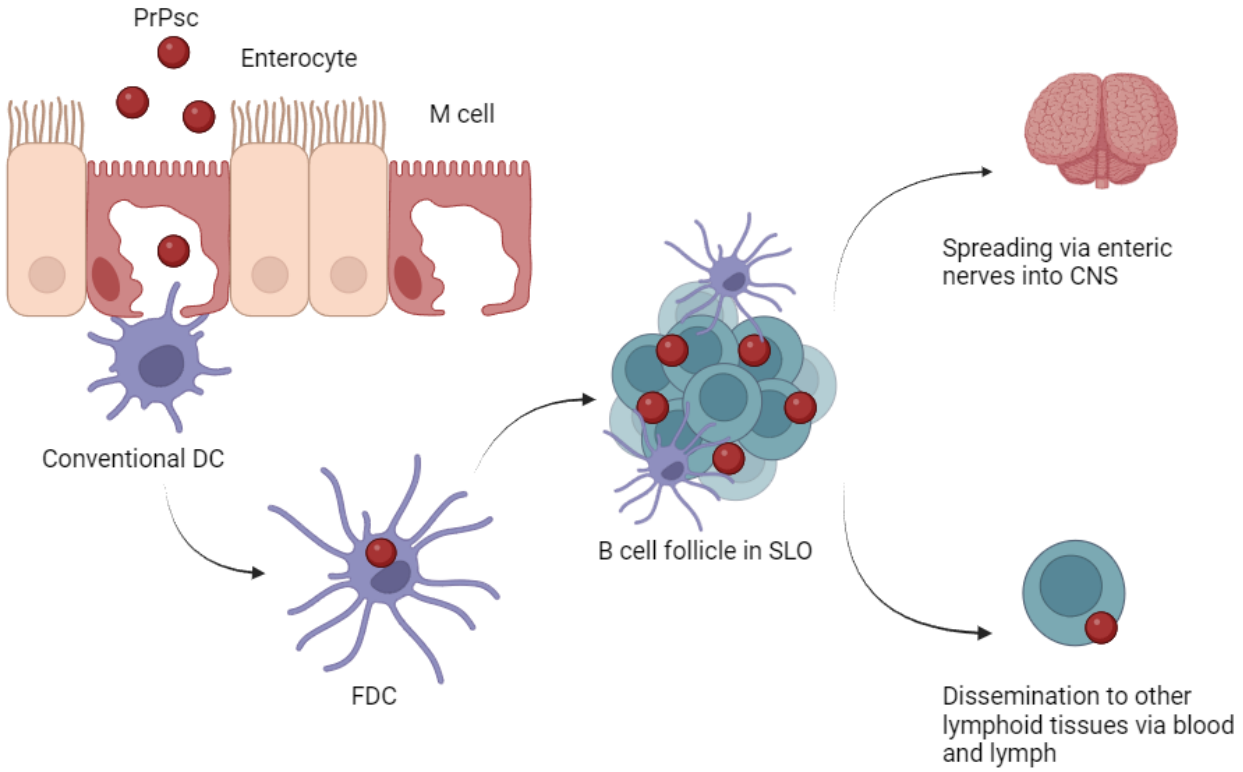

Figure 4. Page 9. Illustration of the spread of prions from the intestine to the central nervous system. Prions must cross the gut epithelium via M cells and are delivered to FDC by conventional DC. After oral exposure of prions, PrPsc accumulates first in the SLO, and the replication of PrPsc happens upon FDC within the B cell follicle, then PrPsc spreads to CNS or other lymphoid tissues.

Diagnosis Approaches

Conventional diagnostic assays for prion diseases include immunohistochemistry (IHC), enzyme-linked immunoassays (ELISA), and Western blot (WB), which are considered the “gold standard” diagnostic approaches for CWD and are popularly applied in clinical CWD diagnosis[30,75]. Novel methods like protein misfolding cyclic amplification (PMCA) and real-time quaking-induced conversion (RT-QuIC) are being developed as potential new diagnostic methods. These methods detect misfolded prion proteins by seeding and the amplification of prion protein in the PrPc-rich medium, allowing the early detection of PrPsc in the disease process[76].

In conventional prion diagnosis, retropharyngeal lymph nodes and obex from the brains of cervids are collected and analyzed. In wild animals, it is difficult to know when they contracted CWD[77]. There is a previous study in which cattle were orally infected with BSE brain tissue and then analyzed at different time points[78]. Study results showed that histopathological features including spongiform change, neuronal loss, astrogliosis, and microgliosis were observed only shortly before the appearance of clinical symptoms (38 months), while immunohistochemical detection of accumulations of PrPsc gave a positive result about six months earlier (32 months). The major limitation of both conventional prion diagnosis and novel methods is not able to perform easily in the field.

Chapter Two

The identification of biomarkers of CWD in white-tailed deer from nasal swabs.

Abstract

Chronic wasting disease (CWD) is a fatal prion disease in the cervid population, and there is no treatment or vaccine for it. CWD has been spreading fast in North America since the 1960s, and it has been reported in 29 states and other countries. Currently, ELISA and Western blot are major methods for CWD diagnosis, whereas these invasive tests can`t be applied in the field and performed post-mortem. So an on-site noninvasive test is urgently needed for CWD susceptible animals. Though the CWD pathogenesis is still elusive, many CWD biomarkers in blood, brain, and lymphoid node tissue have been found and reported. We hypothesized there are biomarkers including differentially expressed genes (DEGs) in the nasal mucosa that can be informative to CWD processes and be useful to diagnose CWD in its early stages. To identify biomarkers of CWD and gain a better understanding of this prion disease`s pathogenesis, we used next-generation total RNA sequencing to identify DEGs from nasal swabs in CWD-infected white-tailed deer compared to control deer. These biomarkers may be further developed as a diagnostic test to identify Chronic wasting disease-infected animals in the preclinical stages.

Introduction

Chronic wasting disease (CWD) is a kind of cervid prion disease or transmissible spongiform encephalopathy (TSE) disease, CWD can infect many species including: mule deer (*Odocoileus hemionus)*, white-tailed deer (*Odocoileus virginianus*) Reindeer (*Rangifer tarandus*), Sika deer (*Cervus nippon*), Moose (*Alces alces*) and Rocky Mountain elk (*Cervus elaphus nelsoni*) are the susceptible target. Animals including beavers (*Genus Castor*)[79], hamsters and meadow voles (*Microtus pennsylvanicus*) [80], and raccoons are also susceptible to CWD due to habitat overlapping. CWD is the only prion disease spreading in free-range animals. The increasing spread of CWD has raised concerns about the potential for increasing human exposure to the CWD agent. The foodborne transmission of bovine spongiform encephalopathy to humans indicates that the species barrier does not completely protect humans from animal prion diseases[81–84]. Currently, CWD has been found in some areas of North America, including Canada and the United States, Norway, and South Korea. In the US, at least 29 states have reported the occurrence of CWD in free-ranging deer and localized infection rates of more than 25 percent since 2000[30]. The spreading of CWD keeps raising public and scientific concerns for the wild animal industry and health industry. To combat the trend from the CWD epidemic to the CWD pandemic, a quick onsite and preclinical diagnosis method is urgently needed to be developed.

Like other prion diseases, CWD is a slowly progressive prion disease, and it usually takes over a year to develop neurological signs. In previous CWD research, CWD diagnosis cannot rely on CWD clinical signs, for some CWD-infected animals (deer and elk) did not show any clinical signs for months or years even after they had been confirmed CWD-positive with tests[85]. As CWD progresses, the infected animals may have a variety of changes in behavior and appearance including drastic weight loss, stumbling, lack of coordination, listlessness, drooling, excessive thirst or urination, drooping ears, and lack of fear of people[84]. It is often difficult to diagnose a deer, elk, or

moose with CWD only based on these symptoms alone because many CWD symptoms also occur with other diseases and malnutrition. Conventional CWD diagnosis methods are immunohistochemistry (IHC), enzyme-linked immunoassays (ELISA), and Western blot (WB). They are all invasive diagnostic tests (taking infected tissue from animal post-mortem) and are not suitable for onsite preclinical CWD diagnosis.
In the previous research, nasal brushes from the CWD white-tailed deer tested earliest positive at 15 MPI by RT-QuIC, but the accuracy was only 56% [86], and for the elk nasal brushings the sensitivity of RT-QuIC was low (34%)[87]. PrPsc was accumulated and detected in lymphoid tissues in the early CWD stage; in the advanced CWD stage, PrPsc was confirmed in the brain tissue[88,89]. However, there was no report of PrPsc existing in the nasal tissue of CWD, PrPsc or PrPsc shred was detected in the olfactory system (OS) in other prion diseases (scrapie, CJD, and BSE)[90–94]. This provides the rationale and the possibility of using nasal swabs as an onsite diagnostic approach for CWD.

In this study outlined in **Figure 5**, we used next-generation total RNA sequencing to identify differentially expressed genes (DEGs) from nasal swabs collected from white-tailed deer. We identified 438 genes differentially expressed in 9 MPI, 12 MPI, and 15 MPI. The identified DEGs may be useful biomarkers to develop an antemortem CWD diagnostic method using nasal swabs.

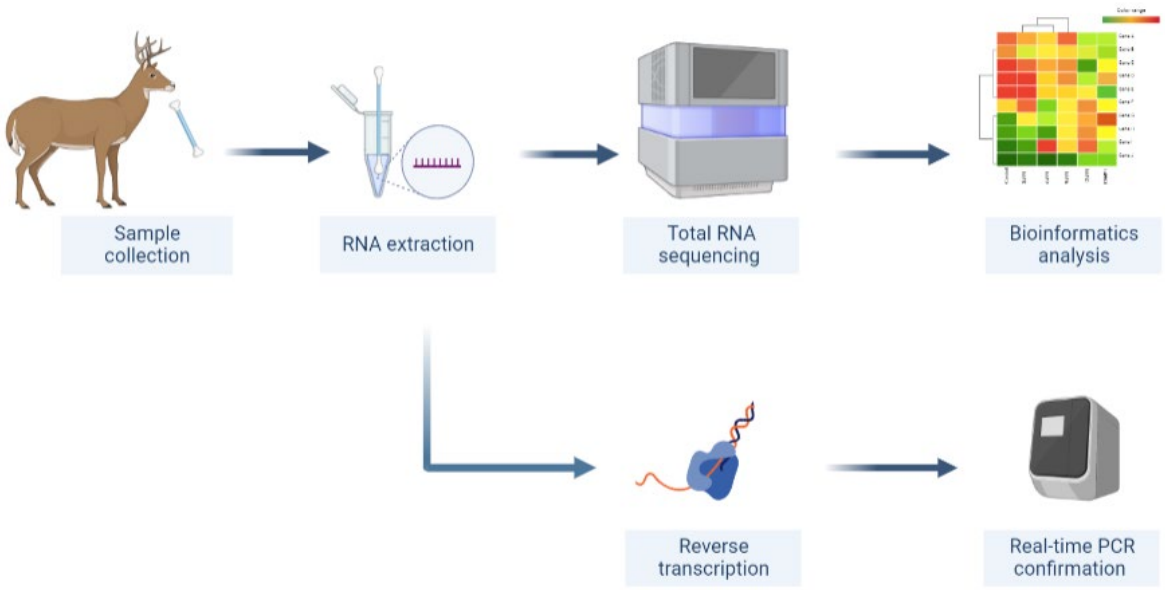

Figure 5. Page 14. Identification of DEGs in nasal swab samples from CWD-infected white-tailed deer. First, nasal swab samples were collected from inoculated and non-inoculated deer. Then total RNA was extracted from nasal swab samples by RNA extraction kits. Bioinformatics analysis was performed with total RNA sequencing results of selected samples to identify DEGs (fold change over 2). In the last, the fold changes of DEGs were further confirmed by RT-PCR.

Materials and Methods

Animal CWD infections

Animal infections were done by Dr. Greenlee`s lab at the Virus and Prion Research Unit at the USDA, National Animal Disease Center in Ames Iowa. White-tailed deer were used for CWD infection. One animal in each room was inoculated by the oronasal route with 1 ml of 10% brain homogenate (0.1g of brain tissue). Each inoculated animal is of the wild-type PRPc genotype (QQ95 GG96 QQ226). The IDs of those animals were 1905, 1944, 0-39, 1904, B-167, B-166, 1945, 1942, 1941, and 1901. Two non-inoculated sentinel deer were placed in each room with a single inoculated deer.

Nasal Swab samples collection

Each sample was collected with a brush (SnapTip Cervical brush (SPH500-CDI, Cancer Diagnostics, Inc). The brush was gently inserted into the nasal vestibule directed dorsocaudally through the dorsal nasal meatus and advanced 6-7 inches until located rostral to the ethmoid turbinate. The brush was swirled gently to collect tissues and mucus. To preserve the sample, the brush was swirled in a prefilled RNAShield brush tube (ZymoResearch, R1109).

RNA purification, library preparation, and sequencing

Total RNA was isolated from the RNAShield nasal brush samples using a commercial kit, following the manufacturer's instructions (Zymo Quick Miniprep Plus kit (R1057, R1058)). RNA quality was assessed via spectrophotometry (NanoDrop Technologies, Inc.) and gel electrophoresis (Bioanalyzer 2100, Agilent Technologies) by the University of Minnesota Genomics Center (UMGC). The UMGC experts performed QC, library construction, and sequencing. Total eukaryotic RNA isolates are quantified using a

fluorimetric RiboGreen assay. Total RNA integrity is assessed using capillary electrophoresis (Agilent BioAnalyzer 2100), generating an RNA Integrity Number (RIN). For samples to pass the initial QC step, they need to quantify higher than 200 nanograms and have a RIN of 7 or greater, then they are converted to Illumina sequencing libraries. Total RNA samples are converted to Illumina sequencing libraries using Illumina Stranded Total RNA Prep Ligation with Ribo-Zero Plus kit (cat#: 20040525). A normalized input mass of total RNA is enzymatically depleted of rRNA using sequence-specific Ribozero capture probes. The reduced RNA is then fragmented and reverse transcribed (via random hexamers) into cDNA and then undergoes second-strand synthesis. The resulting cDNA fragments are blunt-ended, adenylated, and ligated to universal pre-index anchors. A final PCR amplification enriches the anchor-ligated DNA fragments and incorporates primer sequences for cluster generation and unique barcodes for each library. The final library size distribution is validated using capillary electrophoresis and quantified using fluorimetry (PicoGreen). Indexed libraries are then normalized, pooled, and size selected to 320 bp (tight) using the PippinHT instrument to generate libraries with average inserts of 200 bp. Pooled libraries are denatured and diluted to the appropriate clustering concentration. The libraries are then loaded onto the NovaSeq paired end flow cell and clustering occurs on board the instrument. Once the clustering is complete, the sequencing reaction begins using Illumina’s 2-color SBS chemistry. Upon completion of read 1, 2 separate eight-base pair index reads are performed. Finally, the clustered library fragments are re-synthesized in the reverse direction thus producing the template for paired end read 2. Base call (.bcl) files for each cycle of sequencing are generated by Illumina Real Time Analysis (RTA) software. The base call files and run folders are streamed to servers maintained at the Minnesota Supercomputing Institute. Primary analysis and de-multiplexing are performed using Illumina’s bcl2fastq v2.20. The end result of the bcl2fastq workflow is de-multiplexed FASTQ files that are released to Skinner lab`s account for subsequent analysis by following mapping software and aligner.

Sequence read alignment to reference genomes

Following sequencing and raw reads were inspected for quality using FastQC and MultiQC by UMGC in UMN. Reads were aligned to the Ovir.te_1.0 genome and raw counts were calculated using the CHURP-PURR pipeline by Dr. Natalia Calixto Mancipe. From the 31,579 annotated genes in the reference genome, 28,057 genes were identified. Genes with less than 300 bp or less than ten counts per million in at least one treatment group were excluded from the downstream analysis. The filtered dataset contained data from fourteen adult deer (five males and nine females) over six different time points (0, 3, 6, 9, 12, and 15 months post-inoculation, MPI) and 18,383 genes.

Data exploration and differential gene expression

To estimate the effect of time post-inoculation with CWD-inducing prions, gene expression was modeled by Dr. Natalia Calixto Mancipe with a generalized linear model using the edgeR package. Deer, batch, and month were used as explanatory variables. Differential expression was assessed using a quasi-likelihood test on the model and the FDR < 0.05 threshold. I produced a list of genes that were consistently differentially expressed between 9, 12, and 15 MPI and the baseline timepoint (0 MPI). Samples were clustered using the log2-transformed counts per million (CPM) with a pseudocount of 1 for these biomarkers using an unsupervised hierarchical approach.

Quantitative real-time PCR validation

Total RNA samples were used for quantitative real-time PCR. Total RNA extracted from five animals (five pre-inoculated nasal swab samples and five 12 MPI nasal swab samples) were reverse transcribed to cDNA using the SuperScript IV kit (Cat# 18090050). A CFX96 Real-Time instrument (Bio-Rad) and iTaq Universal SYBR Green

Supermix (Bio-Rad) were used following the manufacturer's instructions. PCR primers were designed using NCBI primer designing tools and the Primer Bank website. PCR Primers either spanned introns or included an exon junction. The annealing temperature was 58 °C for all reactions. cDNA prepared from white-tailed deer brain, lymphoid node, and tongue samples was used to optimize primers and to produce standard curves. Brain tissue was obtained from hunter-harvested white-tailed deer (Wisconsin, CWD test negative); tongue tissue and lymphoid nodes were obtained from white-tailed deer hunted by Negin Goodarzi in Oxbow Park and Zollman Zoo. Each target had two reactions without a template gene as negative controls. 25ng cDNA for each sample was added in each PCR well, and β-actin was used as the reference gene.

Results and Discussion

In order to acquire nasal swab samples from CWD-infected and the control group of white-tailed deer, we collaborated with Dr. Justin Greenlee at the Virus and Prion Research Unit at the USDA National Animal Disease Center. Dr. Greenlee's team infected animals and collected samples for our studies. All the deer were born from 5/15/2019 through 7/15/2019 and thus were of similar age. Each inoculated deer was put in one individual room and was inoculated by the oronasal route with 1 ml of 10% brain homogenate (0.1g of brain tissue). Two non-inoculated "sentinel" deer were cohoused with one inoculated deer in the room. **Table 1** shows the cohort of animals included in this study and indicates the time at which animals tested positive for PrPsc via rectal biopsies and when they developed clinical symptoms. All inoculated deer had positive rectal biopsies and developed clinical signs except for 1941 and 1901. 1941 developed clinical signs without ever showing detectable PrPsc in rectal biopsies PrPsc in 1901 is currently non-detectable. Detected clinical signs included loss of condition, head tremor, muscle fasciculations, uncoordinated stumbling, difficulty rising, teeth grinding, hypersalivation, and polydipsia. A few deer were observed to have regurgitated rumen contents. For this study, we extracted RNA and sequenced 51 nasal swab samples in total; the details of these animal samples are listed in **Table 1**.

	Animals IDs	Sex	Genotype	Before inoculation (0MPI)	3 MPI	6 MPI	9 MPI	12 MPI	15 MPI	CWD - positive by RB (MPI)	Survival Time (MPI)
Inoculated deer	1944	Female	kk	✓	✓	✓	✓	✓	✓		23
	1941	Male	GG	✓	✓		✓	✓	✓	12	
	O39	Female	GG	✓	✓				✓	6	19
	1901	Female	GG	✓			✓	✓			
	B166	Female	GG	✓			✓	✓	✓	9	18
	1904	Female	GG	✓	✓	✓	✓	✓	✓	24	33
	1945	Male	GG		✓	✓	✓		✓	6	20
	1942	Male	GG		✓	✓	✓		✓	24	33
	B167	Female	GG			✓	✓			3	21
	1905	Female	GG	✓	✓	✓		✓		12	13
Non-inoculated deer	1943	Male	GS	✓							
	Y15	Female	SK	✓ -							
	Y16	Female	SK	✓ -							
	1946	Male	GS	✓							
	B119	Female	KK	✓							
	B204	Female	QH/GS	✓ -							
	B120	Female	KK	✓							
	O37	Female	QH/GS	✓ -							
	B206	Female	QH/GS	✓ -							
	Y18	Female	SK	✓ -							

Table. 1 Page 20. Animal cohort information. PRNC genotype is indicated. Check marks indicate samples used and sequenced for this study. Subtract marks indicated that they were not used for the following analysis. The time PrPsc was first detected via rectal biopsies and the time of onset of clinical symptoms are listed.

According to Dr. Greenlee`s analysis of PrPsc in rectal biopsies, the first CWD clinical signs were observed at 13 MPI (on average 22.5 MPI).

To identify differentially expressed genes (DEGs) in CWD nasal swab samples, we extracted RNA and sequenced each sample (**Table 1**). We compared results from the CWD samples and control samples. We sequenced nasal swab samples in two batches: with the non-infected sentinel group, 0 MPI and 12 MPI in the first batch; and 3 MPI, 6 MPI, 9 MPI, and 15 MPI in the second batch. Nine pre-inoculation samples from

the first batch were added and re-sequenced with the second batch to help reduce the batch effect.

All RNA used for sequencing library prep was of high quality (RIN score > 7). RNA sequencing generated 136,186,543 mean read-pairs per sample for the first batch and an average of 80,032,453 read-pairs per sample for the second batch.

B204, B206, O37, Y15, Y16, and Y18 were not used in the differential gene expression analysis, because there were many others with the same attributes (female, non-inoculated) and with more than one sequencing result which could control individual variation for the following analysis. Non-inoculated samples 1943, 1946 B120, and B119 were used in the differentially expressed gene analysis. All inoculated samples were used in the differentially expressed gene analysis.

As an exploratory experiment, principal component analysis (PCA) analysis was done first based on sequencing results in order to visualize the massive gene data. According to the PCA graph, PC1 seems to correlate with time, which indicates gene expression was different at each time point. Of interest, one pre-inoculated animal (1905-pre) did not cluster closely with other CWD-deer samples in the PCA plot (**Figure 6**). But there were objective reasons such as the sample`s RIN score being higher than seven and it passed the sequencing QC check to justify removing this animal as an outlier. Given this, 1905-pre was maintained in the analysis.

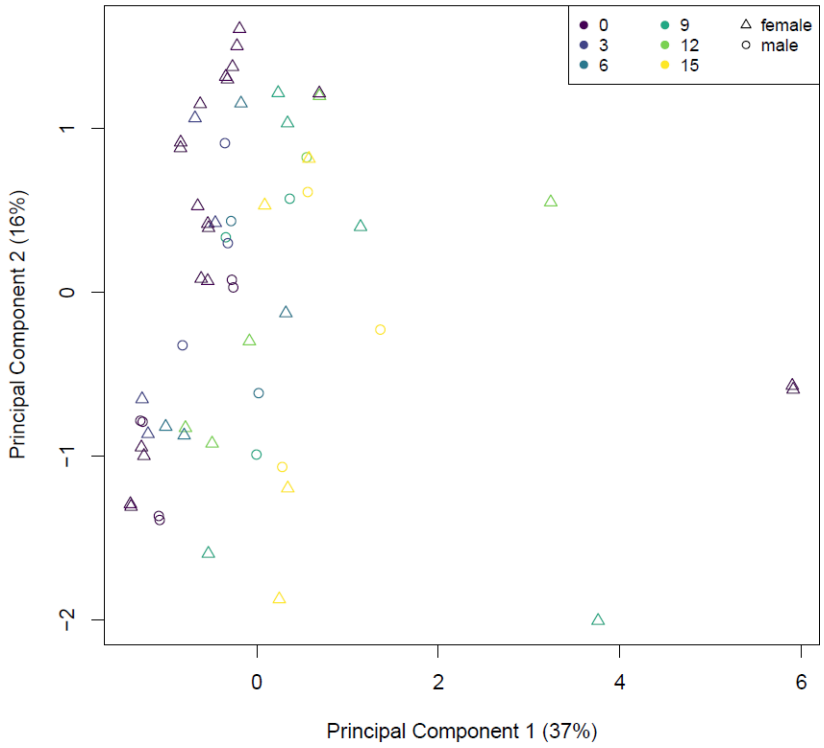

Figure 6. Page 22. Principal component analysis (PCA). Gene expression data from each sample was transformed by projecting each expression measure onto two principal components.

To identify CWD biomarkers, we performed differential gene expression analysis using the edgeR package and compared the day 0 inoculated and non-inoculated animals to each time point collected post-infection. We identified 160 suppressed genes and 159 upregulated genes at three-month post-infection (MPI), 70 suppressed genes and 53 upregulated at 6 MPI, 641 suppressed genes and 1109 upregulated at 9 MPI, 431 suppressed genes and 485 upregulated at 12 MPI, 1454 suppressed genes and 855 upregulated at 15 MPI (**Figure 7A**). There was no gene identified to be significantly differentially expressed (FDR p-value < 0.05) at all the time points post-infection. However, 438 DEGs were found consistently altered at 9 MPI, 12 MPI, and 15 MPI

(**Figure 7B**). R and package EdgeR were used to generate a heat map of the 438 DEGs (**Figure 8**). This analysis plot indicated the difference in each gene expression for all animals. The 9-12 MPI samples clustered together and showed distinct expression patterns compared to the 0-6 MPI samples.

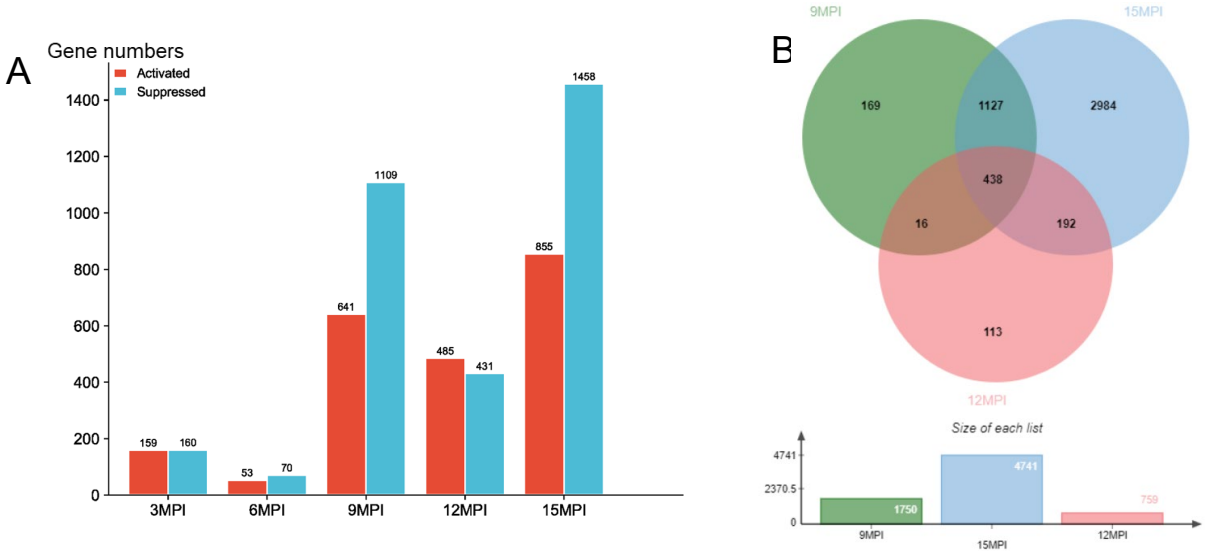

Figure 7. Page23. DEGs at different MPIs. A) In the DEGs (FDR-P< 0.05) histogram, the red bar indicates upregulated genes, and the blue bar indicates the suppressed genes; B) 438 DEGs were consistently differentially expressed at 9 MPI, 12 MPI, and 15 MPI.

Table 2. Page 23. Details of 438 DEGs identified at 9, 12, and 15 MPI can be found at this link:
https://docs.google.com/https://docs.google.com/spreadsheets/d/18J91QfMIrBP1CGZCkApMeCK5zzTXrcElMT0B7accCLY/edit#gid=0spreadsheets/d/18J91QfMIrBP1CGZCkApMeCK5zzTXrcElMT0B7accCLY/edit#gid=0

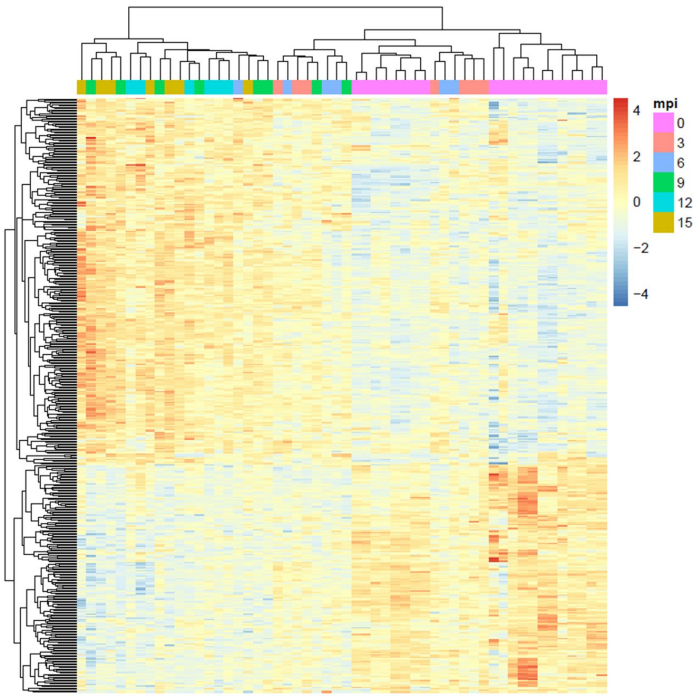

Figure 8. Page 24. Heat map of 438 DEGs identified at 9, 12, and 15 MPI. Among these DEGs, 270 genes were upregulated, and 168 genes were suppressed. The color bar indicates the result of log2-transformed counts per million of the biomarker genes with bright red being highly upregulated and dark blue being highly downregulated. Color blocks indicated the MPI of each sample.

In order to visualize the “relationship” between samples at different time points, we performed a DESeq2 heat map analysis. This analysis plots indicated the similarity between different samples; the red color means similar, and the blue color means different. The results of this analysis are shown in **Figure 9**. The 0 MPI and 3 MPI clustered well which means their gene expression profiles were similar. The 9-15 MPI clustered together and were similar to each other and distinct from 0-3 MPI samples.

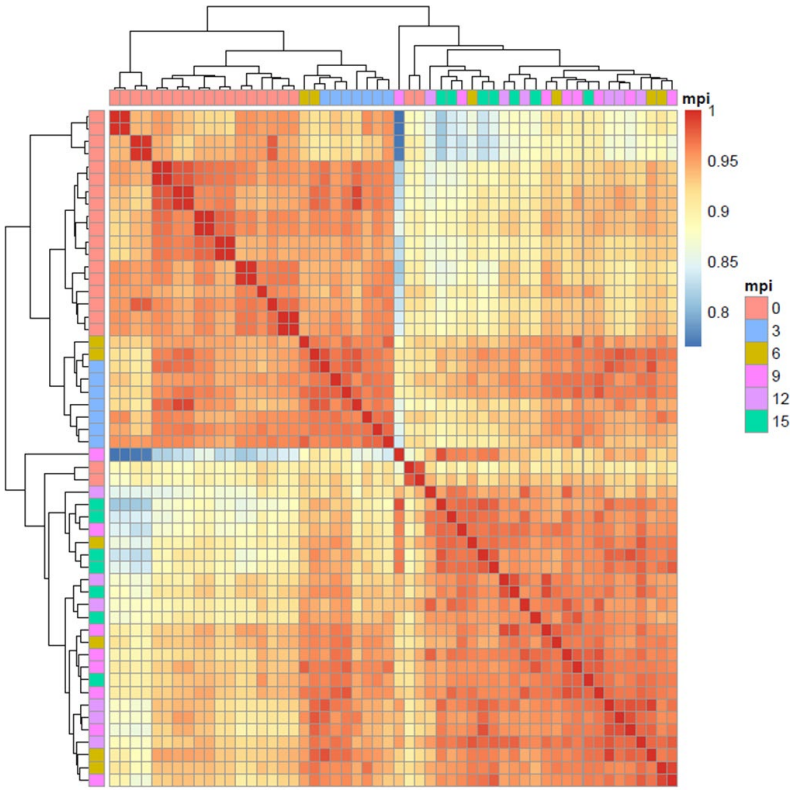

Figure 9. Page 25. Samples` similarity map. This graph based on gene expression level shows the correlation among different time point samples; color indicates the similarity of samples.

9MPI		12MPI		15MPI	
GeneName	logFC	GeneName	logFC	GeneName	logFC
BPIFB6	3.726152	LOC110139672	4.273077	LOC110139672	5.298167
CDSN	3.672675	BPIFB6	3.991596	TCHHL1	4.505498
LOC110144796	3.214459	CDSN	3.798169	LAMB4	4.194274
IL1F10	2.963496	ALOX12B	3.690461	LOC110139878	4.132271
LOC110138206	2.840836	CUNH6orf15	3.647425	LOC110144796	3.943985
TCHH	2.748246	TMEM132C	3.481444	AARD	3.928279
TMEM132C	2.695537	LOC110144796	3.276501	LOC110125863	3.833172
MMP12	2.60523	LOC110146968	3.254764	CDSN	3.409969
LOC110124620	2.510545	PNOC	3.174291	LOC110140010	3.362876
LOC110128424	2.423621	LOC110145065	3.166839	LOC110136313	3.337511
LOC110151433	2.300498	LOC110138206	3.046223	FGF7	3.291492
LOC110145891	2.234815	LOC110139667	3.032423	IL1F10	3.181036
HEPACAM	2.220547	TCHHL1	2.968084	TCHH	3.137729
IL36A	2.213862	ADAMTS16	2.968036	LOC110124620	3.109523
TF	2.14164	LOC110122249	2.96469	LOC110151433	3.105815
LOC110152697	2.016223	LOC110125343	2.902223	CLDN17	3.094335
LOC110152698	1.924141	KLK14	2.868961	KRT1	3.053363
TCN1	1.90419	LOC110139836	2.851761	LOC110135462	3.03545
ATP12A	1.882394	TFPI	2.850092	LOC110145891	3.027435
SERPINB7	1.877551	LOC110123893	2.783709	IL31RA	2.9469
HUNK	-1.65489	LBX1	-2.55605	LOC110132055	-3.62474
CDC20	-1.65682	LOC110152205	-2.55947	LBX1	-3.6365
LINGO1	-1.68499	DDN	-2.60285	NWD2	-3.65682
SIGLEC1	-1.74489	FNDC9	-2.66656	LOC110126572	-3.70055
LOC110122862	-1.78143	XIRP1	-2.6768	GABRR3	-3.70379
ANK2	-1.9281	OC90	-2.7237	GRK1	-3.71532
YPEL1	-2.03453	EN2	-2.74725	LOC110140564	-3.7225
LOC110138007	-2.07688	ROBO3	-2.7584	LOC110139578	-3.73157
IFI6	-2.28974	PTPN5	-2.7857	LOC110122263	-3.74326
ANKRD33	-2.36459	POU3F2	-2.80412	DNMT3L	-3.80029
E2F7	-2.37096	LOC110152291	-2.81424	GNG3	-3.80052
NXPH4	-2.48582	DNMT3L	-2.93862	EN2	-3.81644
FLRT1	-2.53235	CELF5	-3.02916	TAAR1	-3.82811
LOC110141763	-2.55137	ZAN	-3.04559	LOC110131624	-3.86411
LOC110152291	-2.63909	CPLX3	-3.19774	ZAN	-3.91724
DDN	-2.77916	LOC110133984	-3.40473	OBP2A	-4.03561
OC90	-3.08405	DOK7	-3.47864	POU3F2	-4.22698
CELF5	-3.13426	CPLX2	-3.54179	CPLX2	-4.27797
DNMT3L	-3.34513	LOC110129052	-3.85891	SUSD5	-4.34912
ZAN	-3.66171	TRIM17	-3.96303	NWD1	-4.6356

Table 3. Page 26. Twenty up-regulated DEGs and twenty down-regulated DEGs for 9 MPI, 12 MPI, and 15 MPI showed the highest fold-change. logFC: log (gene fold change).

In order to verify the sequencing results, we performed RT-PCR on a subset of the DEGs identified. To achieve this, we first identified the 20 DEGs with the highest fold change (**Table 3**). Next, we successfully designed primers and performed RT-PCR on eight of these genes. **Table 4&5** shows the primer sequence designed for each gene. We chose five animals (1901, 1904, 1941, 1944, and B166) and compared day 0 to 12 MPI. The 2^(-ddCt) method was used to calculate the fold change in RT-PCR. The results of this analysis are shown in **Figure 10**.

Primer pairs for downregulated genes (below)

Gene	Position	Sequence (5'->3')
AATK	FWD	GGCATCGGGTTCAAGGAGTTTG
	REV	GAGCCCTGTGCCGAGAAGTC
ANK2	FWD	CGTGGCTTCCAAGAGGGGAA
	REV	GTGTCAACCCATCGCGAGTTT
FLRT1	FWD	GCAGCCGGAAAAAGGACGAC
	REV	TCTTTGGCGCGGTAAGGGTT
IFI6	FWD	CGCTCTTCCTGTGTTACCTGCTA
	REV	TTGAGCATCTGTTTTCGTCTTCCTC

Primer pairs for upregulated genes (below)

Gene	Position	Sequence (5'->3')
ATP12A	FWD	TCCTGTGCTGGATCGCGTATG
	REV	ACAGAGCCCAAGTACACGTTGTC
HIGD1A	FWD	GTCCACCTGATCCACATGCGT
	REV	CAGGGAATAGCCCATACCAAGAGTC

TCHH	FWD	AGAATGGGGACTCCACCTCACTAT
	REV	TCTCTGGGTCATTTGGTCTCTGGA
TCN1	FWD	TGCAGCCACAATCCAGTCAAATTC
	REV	ATTCAAGGGTGCCGTCGTAGG

Table 4&5. Page 27-28. Genes and primer design for RT-PCR analysis of DEGs. FWD: forward primer; REV: reverse primer. B-actin was used as a reference gene (FWD: CCATGTACCCTGGCATCGCA, REV: CAGGGGGCGCGATGATCTTTAT).

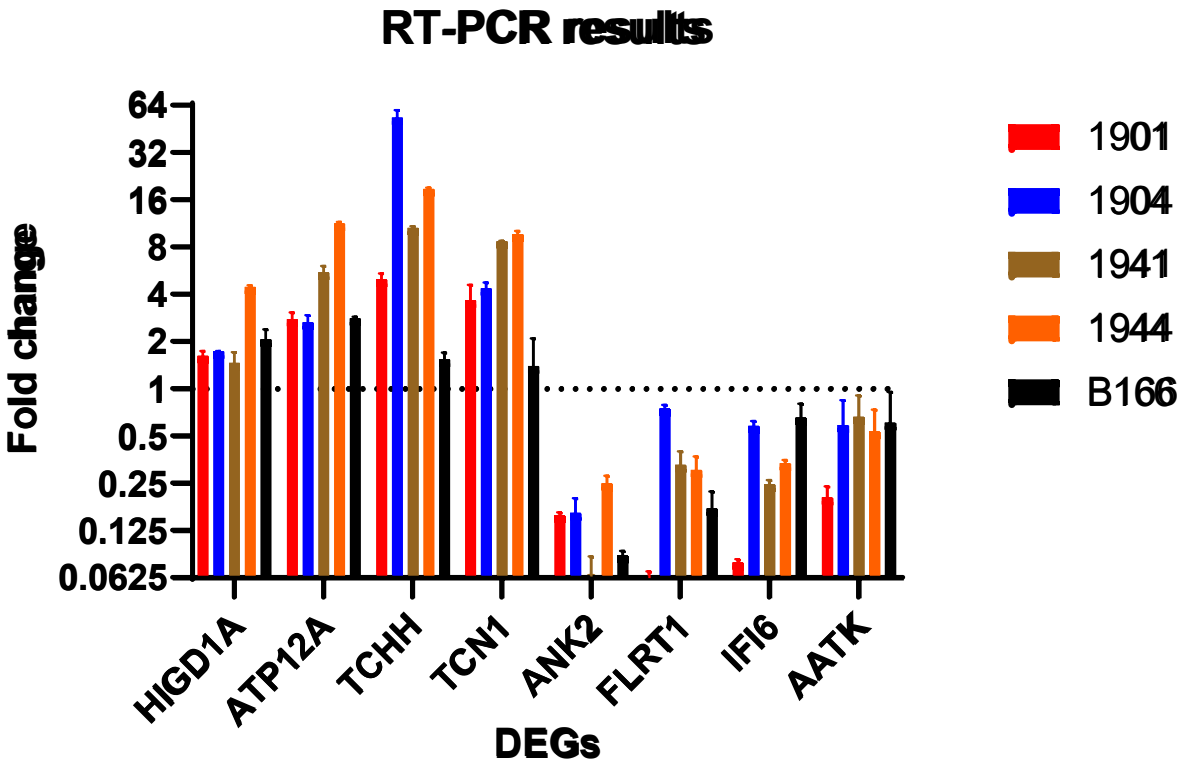

Figure 10. Page 28. RT-PCR results. Expression fold-change between day 0 and 12 MPI are shown in bar height. The bar height above 1 indicates the gene was up-regulated, and the bar below 1 means the gene was down-regulated. Samples were run in triplicate, for n= 3. Error bars represent +/- SD. The equation used to determine fold-change was: ddCt = dCt - dCf; dCt = Ct12 - Ct0; dCf = Cf12-Cf0

fold change = 2^(-ddCt). Ct12: Ct value for 12MPI sample. Ct0: Ct value for 0 MPI sample. Cf12: Ct value for B-actin at 12 MPI group. Cf0: Ct value for B-actin at 0 MPI group.

To fulfill the potential of our findings, we developed a novel readout model (**Figure.11**) based on the identification of biomarkers through total RNA sequencing, which was further confirmed by using RT-PCR. This versatile readout can be adapted for use in a wide range of protein or nucleic acid tests, including antibody tests, RNA/DNA probe tests, and sequencing assays[95–97]. The potential applications of our readout allow it to be deployed in diverse settings, whether it be in remote field locations or well-equipped laboratory facilities, promising significant reductions in testing time and increased efficiency for live animal testing. To ensure its robustness and reliability, we plan to conduct comprehensive validation studies on various animal models, including the CWD- animal model, CWD+ animal model, inflammation animal model, and other neurodegenerative disease animal models (e.g., Alzheimer's disease, Parkinson's disease, or Huntington's disease) in future. In one recent CWD study, a subset (57%) of identified microRNA-biomarkers was found in both CWD positive elk and CWD positive hamsters which indicated that our CWD diagnosis readout might also be able to be applied in different species[98].

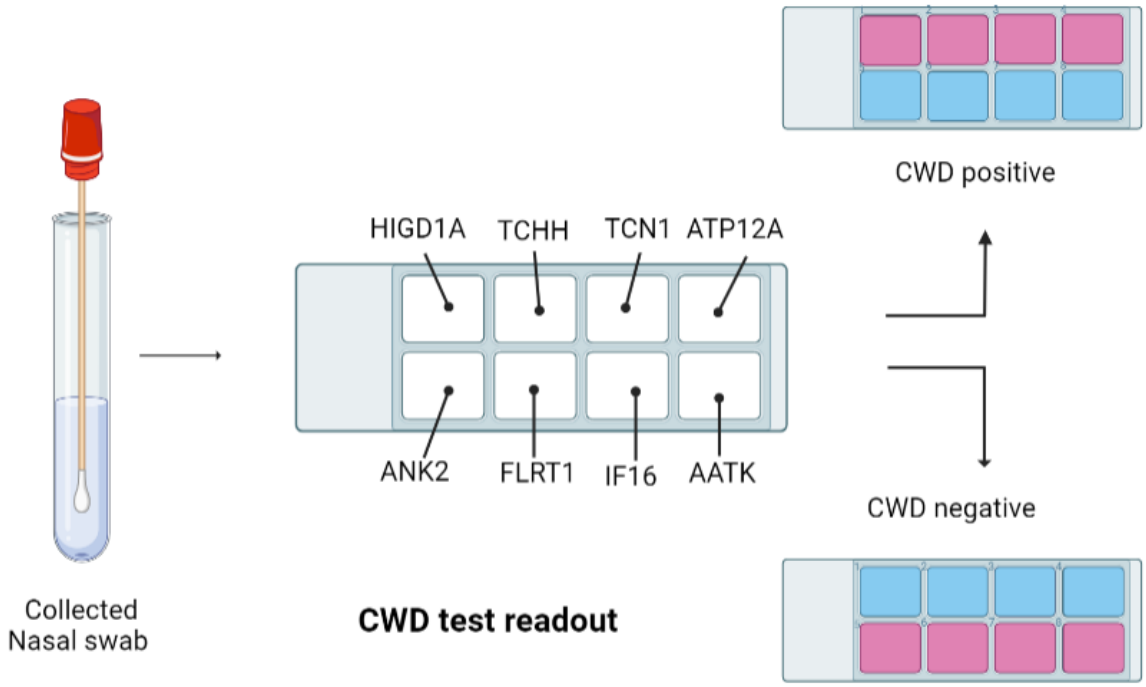

Figure 11. Page 30. Model diagnostic readout based on CWD DEGs. In the upper row are consistently up-regulated CWD genes that show a high fold-change from uninfected animals. The bottom row is consistently down-regulated genes that showed a high-fold change in CWD-infected animals compared to uninfected animals. Red means high concentration, and blue indicates low concentration. If the top row is red and the bottom row is blue, that means the test result is CWD positive; if the bottom row is red and the top row is blue, this would indicate the samples were negative for CWD.

Conclusions

In this research, we identified CWD biomarkers in nasal swabs from CWD-infected animals. These biomarkers are differentially expressed genes detected in nasal swabs from CWD-infected compared to uninfected white-tailed deer. We identified 438 DEGs altered at 9, 12, and 15 MPI. These genes included 270 DEGs that were upregulated, and 168 DEGs were suppressed consistently from 9 MPI to 15 MPI. We successfully designed eight genes` primers and verified their fold change by RT-PCR. Among these eight genes, AATK, ANK2, FLRT1, and IFI6 are four down-regulated DEGs; ATP12, HIGD1A, TCHH, and TCN1 are four up-regulated DEGs.

We designed a novel readout model (**Figure 11**) based on these eight identified DEGs and expected this readout will be applied in a wide range of protein or nucleic acid tests for CWD. We anticipate this preclinical diagnostic test based on a group of nasal swab biomarkers identified here might provide a more rapid, accurate, and reliable assay for CWD. Such assays would need to be validated with CWD-confirmed animals and control animals to determine the feasibility and reliability of this nasal swab biomarker-based clinical assays.

Chapter Three

Insights to CWD Pathogenesis in White-tailed Deer

Abstract

Research on prion diseases has been carried out for more than four decades, but much of prion disease's pathogenesis still remains elusive. In this study, we identified CWD-associated differentially expressed genes (DEGs), and an abundance of genes were annotated at each time point from nasal swabs. In this chapter, I will describe how these annotated genes we identified provide insights into CWD pathogenesis. We found that some gene-associated pathways were consistently suppressed at different CWD infection time points and some biology processes were altered disparately. Thus, these genes identified in this study and the associated pathways that the genes are associated with provide new insights into CWD pathogenesis.

Introduction

Prion diseases have been identified and under extensive research for decades, yet the intricacies of their pathogenesis remain elusive[7,77,99]. In previous research, such as scrapie, BSE, and Creutzfeldt-Jakob disease have been experimentally transmitted and adapted to species like mouse, mink, and hamster, yielding experimental animal models that have proved useful in the study of prion diseases[27,100,101]. Mouse models were used to identify DEGs in the scrapie[102–104]. Recent research about CWD circulating microRNA in elk serum provides more shreds of evidence about the potential of DEGs as CWD noninvasive diagnosis biomarkers[98]. Previous studies with CWD-infected elk and white-tailed deer identified DEGs in blood, lymphoid nodes, and brain tissues [98,105,106]. These studies suggest that prion infection and pathogenesis include DEGs and that DEGs can identify processes and pathways involved in pathogenesis and disease progression. Identification of DEGs in nasal swabs from CWD-infected animals has not been described. As far as we are aware, this is the first study using CWD nasal swabs to identify DEGs and gain an understanding of CWD pathogenesis. Advancements in bioinformatics analysis and genome databases have paved the way for unraveling prion disease pathogenesis[107,108,] and identified genes based on using next-generation sequencing (NGS) in this study provide some new insights into CWD pathogenesis[109].

In the previous prion`s DEGs research, while informative, exhibits certain limitations. Firstly, concentrating solely on DEGs disregards a significant wealth of information encoded in other annotated genes. Secondly, considering the pivotal role of prion infection timing in disease advancement, these studies typically draw comparisons between uninfected and infected states, potentially overlooking vital nuances in disease progression at different time points. In this study, we performed a sequence of bioinformatics assays to reveal insights into CWD pathogenesis at 3 MPI, 6 MPI, 12

MPI, and 15 MPI beyond the exclusive focus on DEGs but the entire annotated genome data.

Using the datasets generated and described in Chapter 2, we performed a number of analyses to try to understand how the annotated genes might be contributing to the CWD pathogenesis and disease progression. These assays included gene set enrichment analysis (GSEA) using hallmark gene sets, gene ontology (GO) term analysis, and KEGG pathway analysis. GSEA is a computational analytical approach for interpreting gene expression data[110,111]. It can determine whether an a priori-defined set of genes shows statistically significant, concordant differences between two biological states (e.g., phenotypes or treatments)[110,111]. The Molecular Signatures Database (MSigDB) is one of the most widely used database resources for gene enrichment analysis. MSigDB includes more than tens of thousands of annotated gene sets that are used within GSEA software [110]. In MSigDB, we used hallmark gene sets for our gene expression analysis. Hallmark gene sets were generated by a computational methodology based on identifying gene set overlaps and retaining genes that display coordinate expression [112] It reduces the redundancy and variation and provides more refined and precise inputs for GSEA analysis compared with other gene sets[112]. GO analysis is based on the Gene Ontology knowledge base which is a resource that includes current scientific knowledge about the functions of genes and gene products (proteins and RNAs) among different species[113,114]. There are three categories of GO: biological process (BP), molecular function (MF), and cellular component (CC). We used GO BP analysis to provide more insight for DEGs related pathways. The structure of GO analysis can be described in terms of a graph, where each GO term is a node. Kyoto Encyclopedia of Genes and Genomes (KEGG) is a famous database for systematic gene function analysis[115]. In this study, KEGG pathway analysis was used to show the DEGs connection with enriched pathways. These analyses revealed the association of DEGs and enriched pathways in CWD nasal mucosa and provide more insights into CWD pathogenesis. According to these analysis results, we found the DEGs identified at different time points involved variably in cell proliferation, reproduction, protein trafficking, and protein modification during the CWD progress.

Materials and Methods

Enrichment analysis of differentially expressed genes

GSEA, GO, and KEGG analysis were performed by Dr. Natalia Calixto Mancipe at the MSI-RIS, UMN. She used the ranked gene list based on the differential expression test results for each time point. The rank metric is -log10(p-value) x sign (log (fold change)). The ranked gene list was compared against the Hallmark gene sets from the MsigDb, using *Bos taurus* orthologs as the background set and the clusterProfiler package. *B. taurus* was originally used to annotate Ovir_te.1.0; hence the gene symbols were appropriate and its orthologs were a good approximation to the deer genome. From the 18383 genes detected in this study, 13,493 were common to both organisms (same symbol). KEGG and GSEA analysis was performed by using R package clusterProfile; R package dplyr; R package tidyverse; R package limma; R package edgeR; R package patchwork; R package viridis, and R package org. Bt.eg.db. The analysis results were visualized by using the R package ggplot.

Statistical analysis approach

The quasi-likelihood test model was performed on differential expression, and the threshold of FDR < 0.05 was considered significant.

Results and Discussion

To have a better understanding of how the DEGs identified and described in Chapter 2 may be contributing to CWD pathogenesis, we performed additional analysis. To further capitalize on our data set, Dr. Natalia Calixto Mancipe performed GSEA assays comparing each time point (3, 6, 12, and 15 MPI) with day 0 controls with all the annotated genes. The results of these analyses are shown in **Figures 12-16**.

Figure 12 shows processes and pathways associated with DEGs identified at 3 MPI. Twenty-one pathways were significantly enriched at 3 MPI; the detailed data are listed in **Table 6**. In **Table 6**, gene sets were ranked by normalized enrichment scores (NES). Notably, at 3 MPI, the E2F pathway, G2M pathway, and mitotic spindle pathway had the top 3 NES and expression-suppressed gene sets. These cell division-related and enriched genes` expression pathways were suppressed, which might indicate at very early stages of CWD, cell division and proliferation were suppressed. Another top enriched suppressed pathway identified is TNF-α via NF-κB. NF-κB pathway induced by the TNF cytokines family is a complex pathway involved in cell survival, proliferation and differentiation, and immune responses. There are also five enriched inflammatory pathways (IF-Gamma response, IF-Alpha response, allograft rejection, complement pathway, and inflammatory response) that were suppressed in CWD-infected animals at 3 MPI. This provides evidence that CWD may suppress cell proliferation and immune responses during the early disease stage. In comparison, the protein secretion pathway, DNA damage response, and hormone response were activated in 3 MPI.

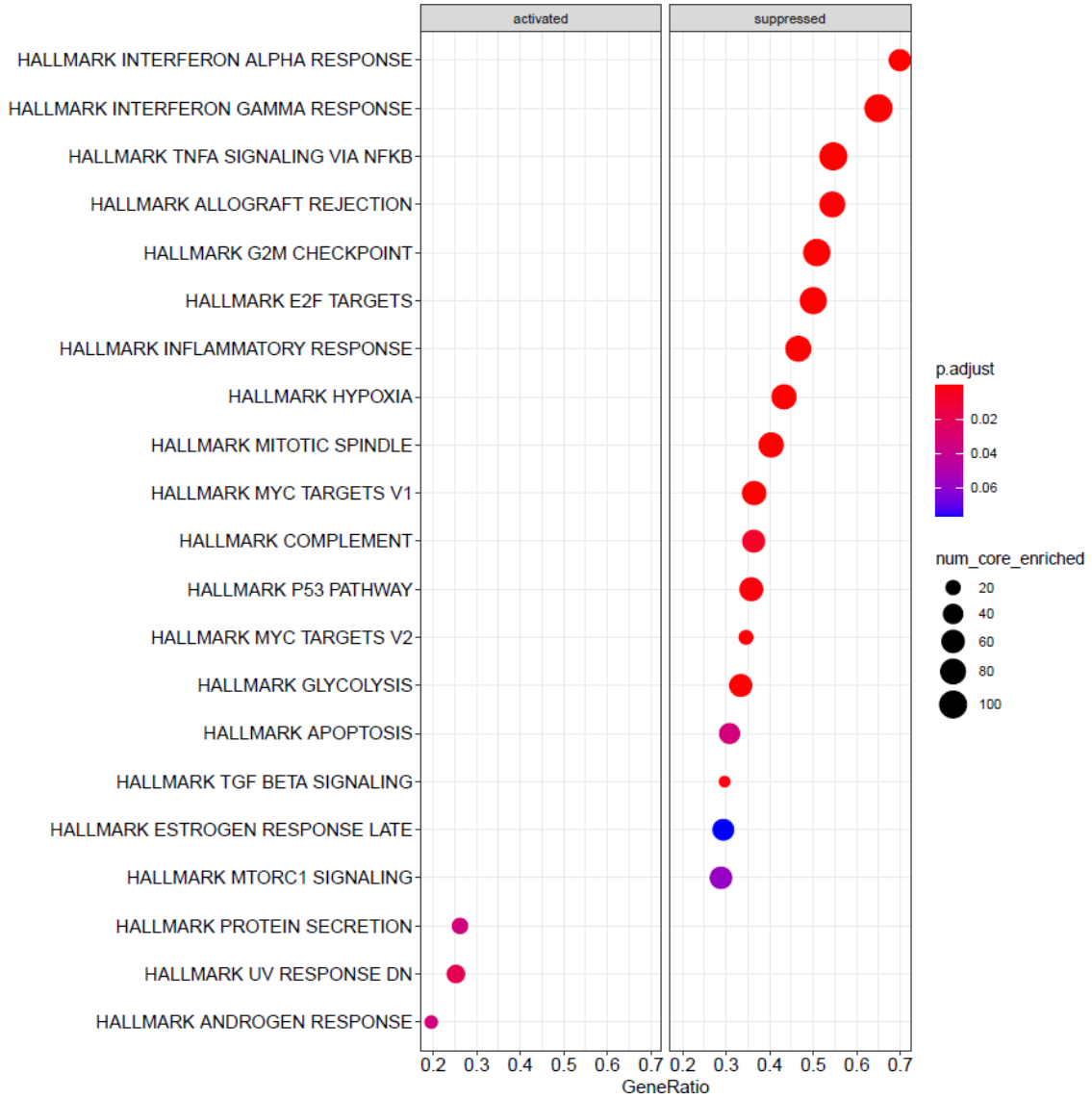

Figure 12. Page 37. GSEA results for 3 MPI. The size of the bubbles indicates the number of enrichment genes in different Hallmark Gene Sets. Spots in the suppressed box mean these gene sets are down-regulated.

ID	setSize	enrichmentScore	NES	pvalue	p.adjust	qvalues	rank	leading_edge	enriched genes
E2F_TARGETS	184	-0.58703	-2.43649	1E-10	2.5E-09	1.53E-09	2280	tags=50%, list=17%, signal=42%	92
G2M_CHECKPOINT	185	-0.63215	-2.62384	1E-10	2.5E-09	1.53E-09	2192	tags=51%, list=17%, signal=43%	94
MITOTIC_SPINDLE	186	-0.50025	-2.07619	9.16E-10	1.53E-08	9.32E-09	2671	tags=40%, list=20%, signal=33%	75
TNFA_SIGNALING_VIA_NFKB	185	-0.50067	-2.07808	1.95E-09	2.44E-08	1.49E-08	3879	tags=55%, list=29%, signal=39%	101
INTERFERON_GAMMA_RESPONSE	157	-0.49235	-1.99988	3.48E-08	3.48E-07	2.12E-07	4008	tags=65%, list=30%, signal=46%	102
INTERFERON_ALPHA_RESPONSE	73	-0.58201	-2.11772	7.16E-07	5.97E-06	3.64E-06	4462	tags=70%, list=34%, signal=47%	51
MYC_TARGETS_V1	184	-0.455	-1.88851	1.29E-06	9.18E-06	5.6E-06	2998	tags=36%, list=23%, signal=29%	67
MYC_TARGETS_V2	55	-0.57261	-1.98232	3.57E-05	0.000223	0.000136	1648	tags=35%, list=12%, signal=30%	19
INFLAMMATORY_RESPONSE	174	-0.4092	-1.68705	7.07E-05	0.000341	0.000208	3565	tags=47%, list=27%, signal=35%	81
GLYCOLYSIS	171	-0.40981	-1.68725	7.09E-05	0.000341	0.000208	2583	tags=33%, list=19%, signal=27%	57
HYPOXIA	171	-0.40944	-1.68575	7.51E-05	0.000341	0.000208	3556	tags=43%, list=27%, signal=32%	74
ALLOGRAFT_REJECTION	149	-0.41644	-1.67997	0.0002	0.000832	0.000508	3892	tags=54%, list=29%, signal=39%	81
P53_PATHWAY	179	-0.39085	-1.6158	0.000351	0.001351	0.000825	2966	tags=36%, list=22%, signal=28%	64
TGF_BETA_SIGNALING	54	-0.50387	-1.73766	0.00072	0.00257	0.001569	2473	tags=30%, list=19%, signal=24%	16
COMPLEMENT	157	-0.37744	-1.53314	0.002189	0.007297	0.004455	3131	tags=36%, list=24%, signal=28%	57
UV_RESPONSE_DN	123	0.34956	1.463813	0.006373	0.019915	0.012159	2046	tags=25%, list=15%, signal=22%	31
ANDROGEN_RESPONSE	87	0.373847	1.48212	0.011579	0.033951	0.020728	1243	tags=20%, list=9%, signal=18%	17
PROTEIN_SECRETION	88	0.370098	1.470104	0.01244	0.033951	0.020728	2646	tags=26%, list=20%, signal=21%	23
APOPTOSIS	143	-0.35065	-1.40659	0.012901	0.033951	0.020728	2764	tags=31%, list=21%, signal=25%	44
MTORC1_SIGNALING	184	-0.32171	-1.33529	0.023346	0.058364	0.035633	2925	tags=29%, list=22%, signal=23%	53
ESTROGEN_RESPONSE_LATE	167	-0.32162	-1.31968	0.032355	0.077036	0.047033	2768	tags=29%, list=21%, signal=24%	49

Table 6. Page 38. GSEA detailed results for 3 MPI. Gene sets were ranked by NES, positive NES indicates this gene set was activated by enriched genes within this gene set; negative NES indicates the gene set was suppressed by enriched genes within this gene set. Set size: the gene component amount for the gene set; enrichment score (ES): the degree to which this gene set is overrepresented at the top or bottom of the ranked list of genes in the expression dataset; normalized enrichment score (NES): ES/mean (ES for all dataset); false discovery rate (FDR) q-value: the estimated probability that the normalized enrichment score represents a false positive finding; rank: the peak position in the ranked list; tag %: the percentage of gene hits the peak; list %: the percentage of genes in the ranked gene list before or after the peak; N: the number of genes in the list; Nh: the number of genes in the gene set; signal%=(tags%)*(1-list%)(N/(N-Nh)).

Thirty-three pathways were significantly enriched at 6 MPI (**Figure 13**), the detailed genes for each pathway are listed in **Table 7**. Notably, according to NES, at 6 MPI, proliferation-related pathways were more down-regulated compared with 3 MPI. NF-κB pathway was more down-regulated compared with 3 MPI as well. The 6 MPI protein secretion pathway was highly upregulated compared with the 3 MPI enrichment result. DNA damage repair pathways were downregulated. The four enriched inflammatory

response pathways were highly suppressed in CWD-infected animals at 6 MPI. Activated pathways at 6 MPI included the Epithelial-mesenchymal transition and angiogenesis pathways.

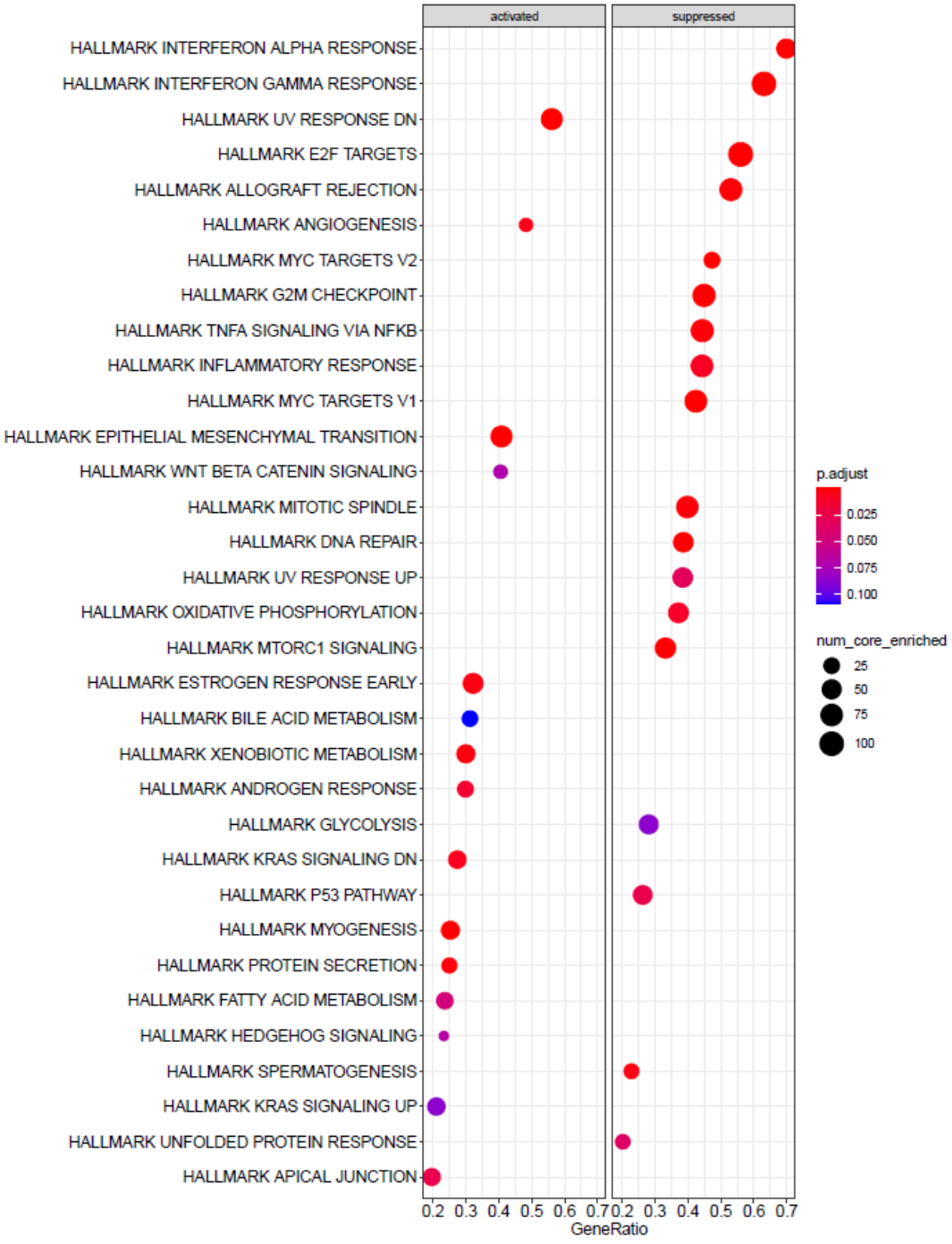

Figure 13. Page 39. GSEA results for 6 MPI. The size of the bubbles indicates the number of enrichment genes in different Hallmark Gene Sets.

ID	setSize	ES	NES	pvalue	p.adjust	qvalues	rank	leading_edge	Enriched gene numbers
E2F_TARGETS	184	-0.694058011	-2.79965	1E-10	1E-09	4.21E-10	2075	tags=56%, list=16%, signal=48%	103
EPITHELIAL_MESENCHYMAL_TRANSITION	169	0.693161012	2.735628	1E-10	1E-09	4.21E-10	1529	tags=41%, list=12%, signal=37%	69
G2M_CHECKPOINT	185	-0.652633009	-2.63275	1E-10	1E-09	4.21E-10	1617	tags=45%, list=12%, signal=40%	84
INTERFERON_GAMMA_RESPONSE	157	-0.562494676	-2.22379	1E-10	1E-09	4.21E-10	3660	tags=63%, list=28%, signal=46%	100
MYC_TARGETS_V1	184	-0.648495156	-2.61586	1E-10	1E-09	4.21E-10	1834	tags=42%, list=14%, signal=37%	78
UV_RESPONSE_DN	123	0.584285768	2.203667	6.61E-10	5.5E-09	2.32E-09	3445	tags=56%, list=26%, signal=42%	69
DNA_REPAIR	140	-0.530937101	-2.0659	8.19E-09	5.85E-08	2.46E-08	2592	tags=39%, list=20%, signal=31%	54
MYC_TARGETS_V2	55	-0.659613834	-2.21582	1.74E-07	1.09E-06	4.57E-07	2307	tags=47%, list=17%, signal=39%	26
INTERFERON_ALPHA_RESPONSE	73	-0.593047962	-2.09511	5.45E-07	3.03E-06	1.27E-06	3543	tags=70%, list=27%, signal=52%	51
MTORC1_SIGNALING	184	-0.404615847	-1.63211	7.92E-05	0.000384	0.000162	2632	tags=33%, list=20%, signal=27%	61
MYOGENESIS	162	0.430934221	1.69295	8.44E-05	0.000384	0.000162	2064	tags=25%, list=16%, signal=22%	41
ALLOGRAFT_REJECTION	149	-0.416776251	-1.63801	0.000268	0.001116	0.00047	3743	tags=53%, list=28%, signal=39%	79
TNFA_SIGNALING_VIA_NFKB	185	-0.393908634	-1.58905	0.000402	0.001548	0.000652	3464	tags=44%, list=26%, signal=33%	82
MITOTIC_SPINDLE	186	-0.387280302	-1.56334	0.000489	0.001742	0.000733	1683	tags=40%, list=13%, signal=35%	74
PROTEIN_SECRETION	88	0.476865029	1.712969	0.000522	0.001742	0.000733	1692	tags=25%, list=13%, signal=22%	22
XENOBIOTIC_METABOLISM	140	0.404194014	1.55447	0.000898	0.002807	0.001182	2251	tags=30%, list=17%, signal=25%	42
ESTROGEN_RESPONSE_EARLY	177	0.384593447	1.525103	0.001303	0.003831	0.001613	2852	tags=32%, list=21%, signal=26%	57
SPERMATOGENESIS	92	-0.443821279	-1.62798	0.001532	0.004255	0.001791	1375	tags=23%, list=10%, signal=21%	21
ANGIOGENESIS	29	0.60946962	1.777931	0.001905	0.005013	0.002111	2512	tags=48%, list=19%, signal=39%	14
KRAS_SIGNALING_DN	135	0.407883756	1.56197	0.003081	0.007701	0.003243	2137	tags=27%, list=16%, signal=23%	37
INFLAMMATORY_RESPONSE	174	-0.361454627	-1.44915	0.003627	0.008636	0.003636	3283	tags=44%, list=25%, signal=34%	77
OXIDATIVE_PHOSPHORYLATION	151	-0.378876776	-1.49208	0.00489	0.011114	0.004679	2971	tags=37%, list=22%, signal=29%	56
ANDROGEN_RESPONSE	87	0.427856078	1.531914	0.00657	0.014283	0.006014	1921	tags=30%, list=14%, signal=26%	26
P53_PATHWAY	179	-0.339605449	-1.36621	0.012455	0.025948	0.010926	2269	tags=26%, list=17%, signal=22%	47
APICAL_JUNCTION	173	0.347286535	1.375199	0.013503	0.027006	0.011371	1614	tags=20%, list=12%, signal=17%	34
UV_RESPONSE_UP	138	-0.351532317	-1.36337	0.016913	0.032526	0.013695	2951	tags=38%, list=22%, signal=30%	53
UNFOLDED_PROTEIN_RESPONSE	99	-0.378841233	-1.4047	0.020412	0.037801	0.015916	1385	tags=20%, list=10%, signal=18%	20
FATTY_ACID_METABOLISM	127	0.354819769	1.345528	0.026832	0.047914	0.020174	2115	tags=24%, list=16%, signal=20%	30
HEDGEHOG_SIGNALING	30	0.505019173	1.486258	0.039395	0.067922	0.028599	1098	tags=23%, list=8%, signal=21%	7
WNT_BETA_CATENIN_SIGNALING	37	0.467006586	1.435338	0.042648	0.071079	0.029928	3019	tags=41%, list=23%, signal=31%	15
GLYCOLYSIS	171	-0.312053121	-1.24758	0.053609	0.086466	0.036407	2877	tags=28%, list=22%, signal=22%	48
KRAS_SIGNALING_UP	171	0.317885299	1.256903	0.055471	0.086674	0.036494	1969	tags=21%, list=15%, signal=18%	36
BILE_ACID_METABOLISM	80	0.364378453	1.292674	0.071633	0.108534	0.045699	2488	tags=31%, list=19%, signal=26%	25

Table 7. Page 40. GSEA detailed results for 6 MPI. Gene sets were ranked by NES; positive NES indicates this gene set was activated by enriched genes within this gene set.

Thirty-two pathways were significantly enriched at 9 MPI (**Figure 14**), the detailed genes for each pathway are listed in **Table 8**. Notably, at 9 MPI, the E2F pathway, G2M pathway, and Mitotic spindle pathway maintained the same suppression level as 6 MPI. The protein secretion pathway was more upregulated in 9 MPI than in 6 MPI. As to immune response pathways, three enriched pathways started to be activated at 9 MPI. But interferon-alpha response pathway and interferon-gamma response pathway remain suppressed as 6 MPI. The estrogen response pathways, cholesterol homeostasis pathway, and adipogenesis pathway were enriched and activated at this time point.

Figure 14. Page 41. GSEA results for 9 MPI. The size of the bubbles indicates the number of enrichment genes in different Hallmark Gene Sets.

ID	setSize	ichmentSc	NES	pvalue	p.adjust	qvalues	rank	ading_edge	Enriched gene numbers
E2F_TARGETS	184	-0.57916	-2.49717	1E-10	2.5E-09	1.05E-09	1362	list=10%, signal=29%	58
G2M_CHECKPOINT	185	-0.5432	-2.34348	1E-10	2.5E-09	1.05E-09	1557	list=12%, signal=29%	59
ESTROGEN_RESPONSE_EARLY	177	0.52595	1.923785	1.52E-08	2.53E-07	1.06E-07	2701	list=20%, signal=32%	70
PROTEIN_SECRETION	88	0.612393	2.061802	2.39E-08	2.99E-07	1.26E-07	3132	list=24%, signal=48%	55
MITOTIC_SPINDLE	186	-0.41765	-1.80139	1.14E-06	1.14E-05	4.82E-06	1672	list=13%, signal=25%	53
FATTY_ACID_METABOLISM	127	0.484633	1.704798	7.98E-05	0.000665	0.00028	3245	list=24%, signal=29%	49
ANDROGEN_RESPONSE	87	0.534213	1.794793	9.66E-05	0.00069	0.00029	3361	list=25%, signal=35%	40
CHOLESTEROL_HOMEOSTASIS	62	0.563575	1.807494	0.000205	0.001283	0.00054	3649	list=27%, signal=41%	35
MTORC1_SIGNALING	184	0.419739	1.53962	0.001298	0.007168	0.003018	1894	list=14%, signal=23%	49
UV_RESPONSE_DN	123	0.450523	1.581683	0.001434	0.007168	0.003018	3065	list=23%, signal=28%	44
OXIDATIVE_PHOSPHORYLATION	151	0.42284	1.520967	0.002073	0.009035	0.003804	3255	list=25%, signal=26%	52
TGF_BETA_SIGNALING	54	0.534092	1.675034	0.002349	0.009035	0.003804	2673	list=20%, signal=30%	20
XENOBIOTIC_METABOLISM	140	0.426832	1.520231	0.002349	0.009035	0.003804	1865	list=14%, signal=19%	31
HEME_METABOLISM	159	0.414426	1.498666	0.002665	0.009518	0.004008	2470	list=19%, signal=26%	51
ADIPOGENESIS	169	0.406421	1.480792	0.003106	0.010354	0.00436	3349	list=25%, signal=28%	63
P53_PATHWAY	179	0.397022	1.45352	0.004397	0.013357	0.005624	2393	list=18%, signal=25%	53
PI3K_AKT_MTOR_SIGNALING	93	0.457612	1.5514	0.004541	0.013357	0.005624	3189	list=24%, signal=32%	39
COAGULATION	107	0.433752	1.496389	0.00737	0.01945	0.008189	2179	list=16%, signal=20%	25
APOPTOSIS	143	0.406055	1.450311	0.007391	0.01945	0.008189	2534	list=19%, signal=23%	40
SPERMATOGENESIS	92	-0.3762	-1.47256	0.009187	0.022967	0.00967	1979	list=15%, signal=24%	26
IL2_STAT5_SIGNALING	178	0.382534	1.39934	0.009769	0.023259	0.009793	3077	list=23%, signal=24%	54
INTERFERON_ALPHA_RESPONSE	73	-0.38491	-1.44789	0.011102	0.025232	0.010624	3184	list=24%, signal=30%	29
PEROXISOME	89	0.437041	1.472935	0.012029	0.026151	0.011011	1782	list=13%, signal=21%	21
ESTROGEN_RESPONSE_LATE	167	0.379933	1.381614	0.014745	0.030718	0.012934	3005	list=23%, signal=29%	61
EPITHELIAL_MESENCHYMAL_TRANSITION	169	0.377482	1.375355	0.016249	0.032497	0.013683	3534	list=27%, signal=25%	57
TNFA_SIGNALING_VIA_NFKB	185	0.367582	1.34922	0.018823	0.036199	0.015241	3598	list=27%, signal=26%	66
MYC_TARGETS_V1	184	-0.28995	-1.2502	0.03009	0.055722	0.023462	1255	list=9%, signal=13%	27
INTERFERON_GAMMA_RESPONSE	157	-0.29635	-1.25393	0.035836	0.063993	0.026944	3201	list=24%, signal=24%	49
REACTIVE_OXYGEN_SPECIES_PATHWAY	47	0.458825	1.404683	0.045192	0.076124	0.032052	2333	list=18%, signal=30%	17
MYOGENESIS	162	0.358226	1.297685	0.045674	0.076124	0.032052	2365	list=18%, signal=19%	37
DNA_REPAIR	140	-0.28874	-1.20434	0.068966	0.111235	0.046836	1174	list=9%, signal=15%	23
HYPOXIA	171	0.343017	1.250511	0.073977	0.115588	0.048669	3297	list=25%, signal=25%	57

Table 8. Page 42. GSEA detailed results for 9 MPI. Gene sets were ranked by NES; positive NES indicates this gene set was activated by enriched genes within this gene set.

Thirteen pathways were significantly enriched at 12 MPI (**Figure 15**) and the detailed genes for each pathway are listed in **Table 9**. At 12 MPI, the E2F pathway, G2M pathway, and Mitotic spindle pathway maintained the same suppression level as 9 MPI. Two immune response pathways were enriched and activated at this time point. The protein secretion pathway was less upregulated in 12 MPI than in 9 MPI.

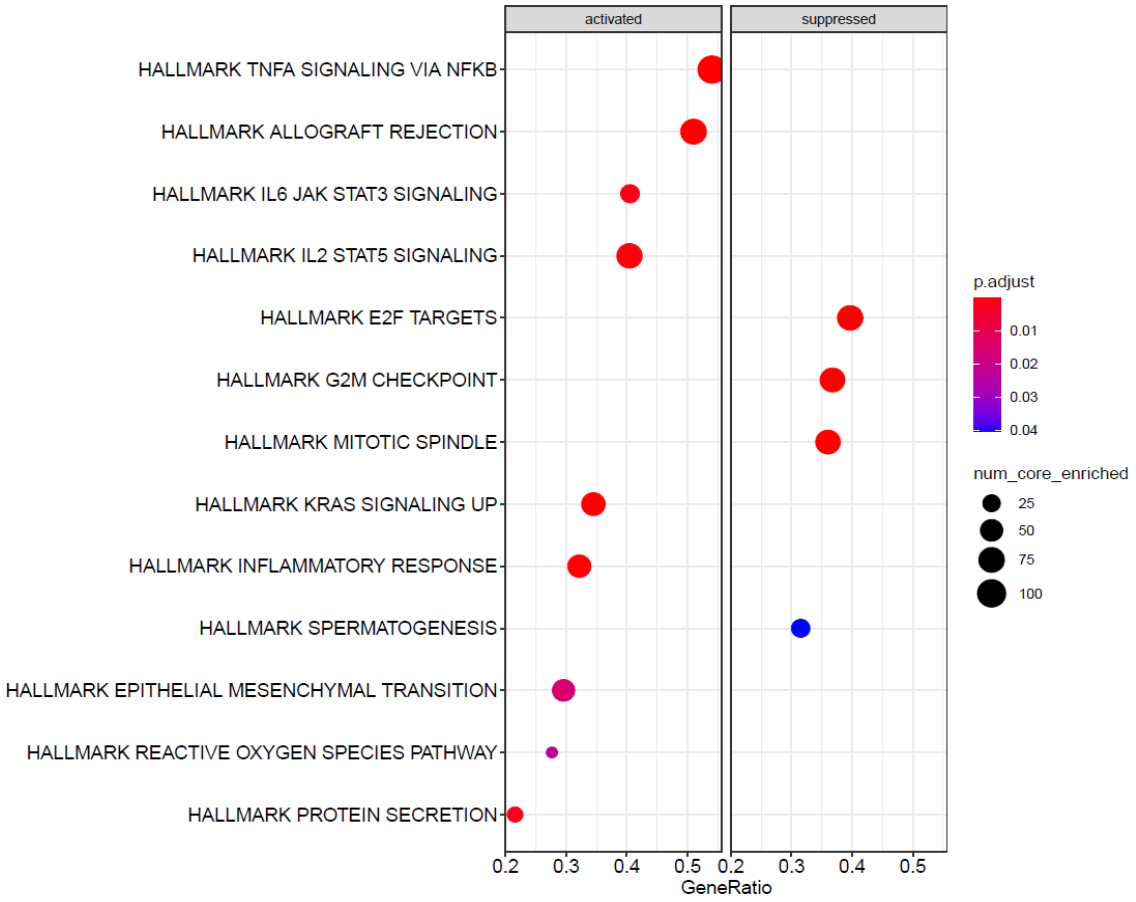

Figure 15. Page 43. GSEA results for 12 MPI. The size of the bubbles indicates the number of enrichment genes in different Hallmark Gene Sets.

ID	setSize	ichmentSc	NES	pvalue	p.adjust	qvalues	rank	leading_edge	Enriched gene numbers
E2F_TARGETS	184	-0.55033	-2.24377	1E-10	1.67E-09	1.05E-09	2321	tags=40%, list=17%, signal=33%	73
G2M_CHECKPOINT	185	-0.55919	-2.28216	1E-10	1.67E-09	1.05E-09	2108	tags=37%, list=16%, signal=31%	68
MITOTIC_SPINDLE	186	-0.53132	-2.17011	1E-10	1.67E-09	1.05E-09	2316	tags=36%, list=17%, signal=30%	67
TNFA_SIGNALING_VIA_NFKB	185	0.542747	2.087152	3.13E-10	3.91E-09	2.47E-09	3831	tags=54%, list=29%, signal=39%	100
ALLOGRAFT_REJECTION	149	0.507816	1.902694	9.73E-07	9.73E-06	6.14E-06	3670	tags=51%, list=28%, signal=37%	76
KRAS_SIGNALING_UP	171	0.468317	1.784934	8.56E-06	7.13E-05	4.5E-05	3001	tags=35%, list=23%, signal=27%	59
INFLAMMATORY_RESPONSE	174	0.451543	1.725302	3.11E-05	0.000222	0.00014	2960	tags=32%, list=22%, signal=25%	56
IL2_STAT5_SIGNALING	178	0.439652	1.684571	0.000107	0.00067	0.000423	3325	tags=40%, list=25%, signal=31%	72
IL6_JAK_STAT3_SIGNALING	74	0.523124	1.775477	0.00037	0.00201	0.00127	3063	tags=41%, list=23%, signal=31%	30
PROTEIN_SECRETION	88	0.491585	1.709486	0.000402	0.00201	0.00127	926	tags=22%, list=7%, signal=20%	19
EPITHELIAL_MESENCHYMAL_TRANSITION	169	0.393779	1.497776	0.003495	0.015887	0.010034	2694	tags=30%, list=20%, signal=24%	50
REACTIVE_OXYGEN_SPECIES_PATHWAY	47	0.526238	1.651541	0.005651	0.023545	0.01487	1335	tags=28%, list=10%, signal=25%	13
SPERMATOGENESIS	92	-0.40083	-1.48556	0.010475	0.040289	0.025446	2330	tags=32%, list=18%, signal=26%	29

Table 9. Page 43. GSEA detailed results or 12 MPI. Gene sets were ranked by NES; positive NES indicates this gene set was activated by enriched genes within this gene set.

Eleven pathways were significantly enriched at 15 MPI (**Figure 16**) and the detailed genes for each pathway are listed in **Table 10**. At 15 MPI, there was no immune response-related pathway enriched. The E2F pathway, G2M pathway, and Mitotic spindle pathway were less suppressed than 12 MPI but still suppressed.

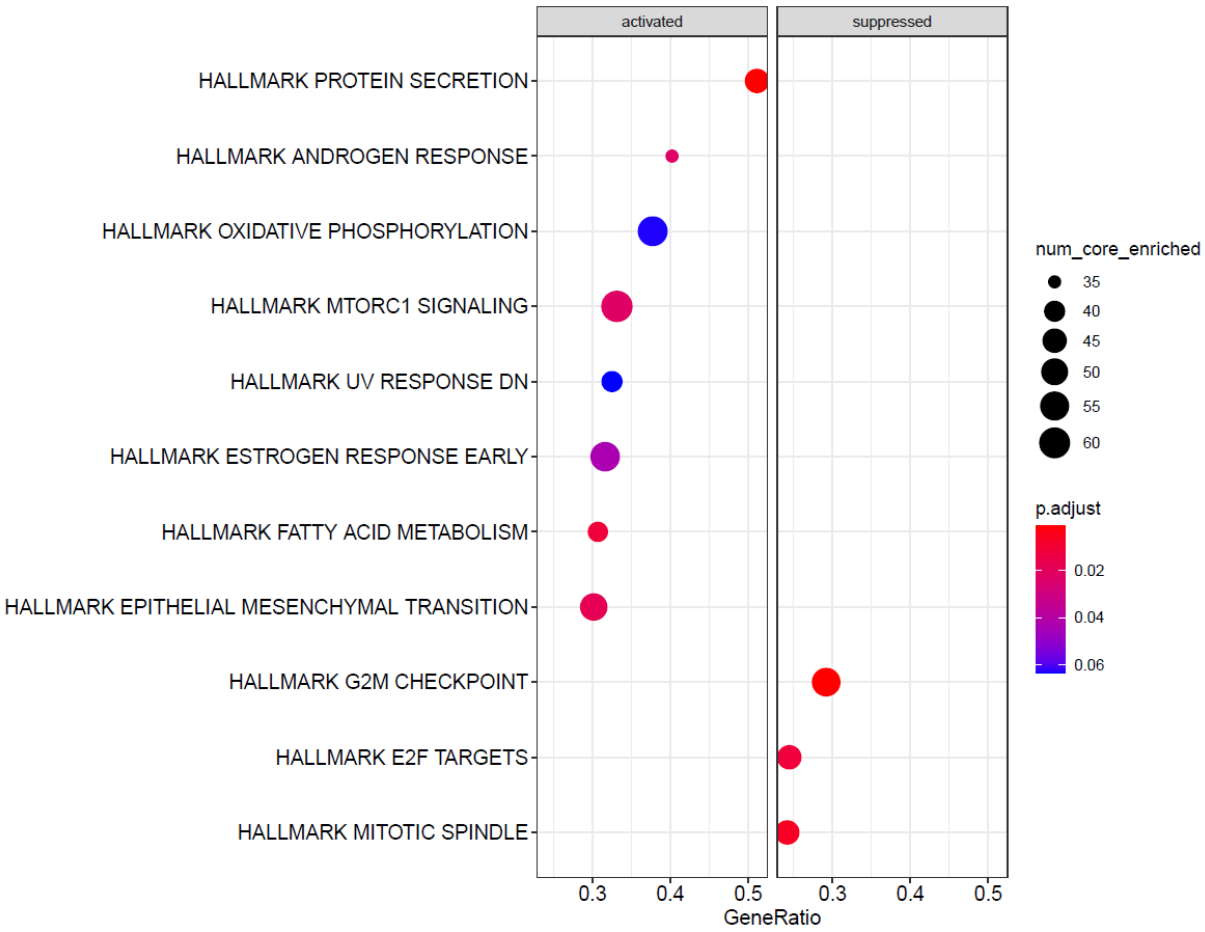

Figure 16. Page 44. GSEA results for 15 MPI. The size of the bubbles indicates the number of enrichment genes in different Hallmark Gene Sets.

ID	setSize	ichmentSc	NES	pvalue	p.adjust	qvalues	rank	ading_edge	Enriched gene numbers
G2M_CHECKPOINT	185	-0.374	-1.65038	3.21E-05	0.001422	0.001048	2370	list=18%, signal=24%	54
PROTEIN_SECRETION	88	0.536081	1.821604	5.69E-05	0.001422	0.001048	3480	list=26%, signal=38%	45
MITOTIC_SPINDLE	186	-0.34308	-1.51503	0.000397	0.006619	0.004877	1653	list=12%, signal=21%	45
E2F_TARGETS	184	-0.34082	-1.50467	0.001031	0.011852	0.008733	2122	list=16%, signal=21%	45
FATTY_ACID_METABOLISM	127	0.440852	1.56743	0.001185	0.011852	0.008733	2323	list=17%, signal=26%	39
EPITHELIAL_MESENCHYMAL_TRANSITION	169	0.404507	1.487277	0.00223	0.018584	0.013693	2995	list=23%, signal=24%	51
MTORC1_SIGNALING	184	0.395124	1.462837	0.003486	0.022622	0.016668	2639	list=20%, signal=27%	61
ANDROGEN_RESPONSE	87	0.461937	1.566255	0.003619	0.022622	0.016668	3049	list=23%, signal=31%	35
ESTROGEN_RESPONSE_EARLY	177	0.384254	1.420212	0.007795	0.043307	0.03191	2779	list=21%, signal=25%	56
OXIDATIVE_PHOSPHORYLATION	151	0.386551	1.404007	0.012564	0.062822	0.04629	3438	list=26%, signal=28%	57
UV_RESPONSE_DN	123	0.399689	1.417957	0.013945	0.063386	0.046706	3143	list=24%, signal=25%	40

Table 10. Page 45. GSEA detailed results for 15 MPI. Gene sets were ranked by NES; positive NES indicates this gene set was activated by enriched genes within this gene set.

In addition to using hallmark gene sets, we also did GO enrichment analysis to understand the CWD pathogenesis. This analysis interpreted the contribution of annotated genes to biological processes at differential time points. In the GO graphs presented in **Figures 17-19**, the size of the plots indicates the gene amount enriched in this pathway and the color red indicates the enriched results are more significant whereas blue indicates less significant. Gene ratio shows the result of the enriched genes in the comparison divided by all the genes in the reference cow genome that composed the pathway. There was no significant enriched biological process detected at 6 MPI.

GO analysis of the DEGs identified at 3 MPI (**Figure 17**) showed five enriched pathways that were cell proliferation-related. These data are supported by the GSEA hallmark gene sets analysis results in which cell proliferation pathways were consistently suppressed from 3 MPI to 15 MPI.

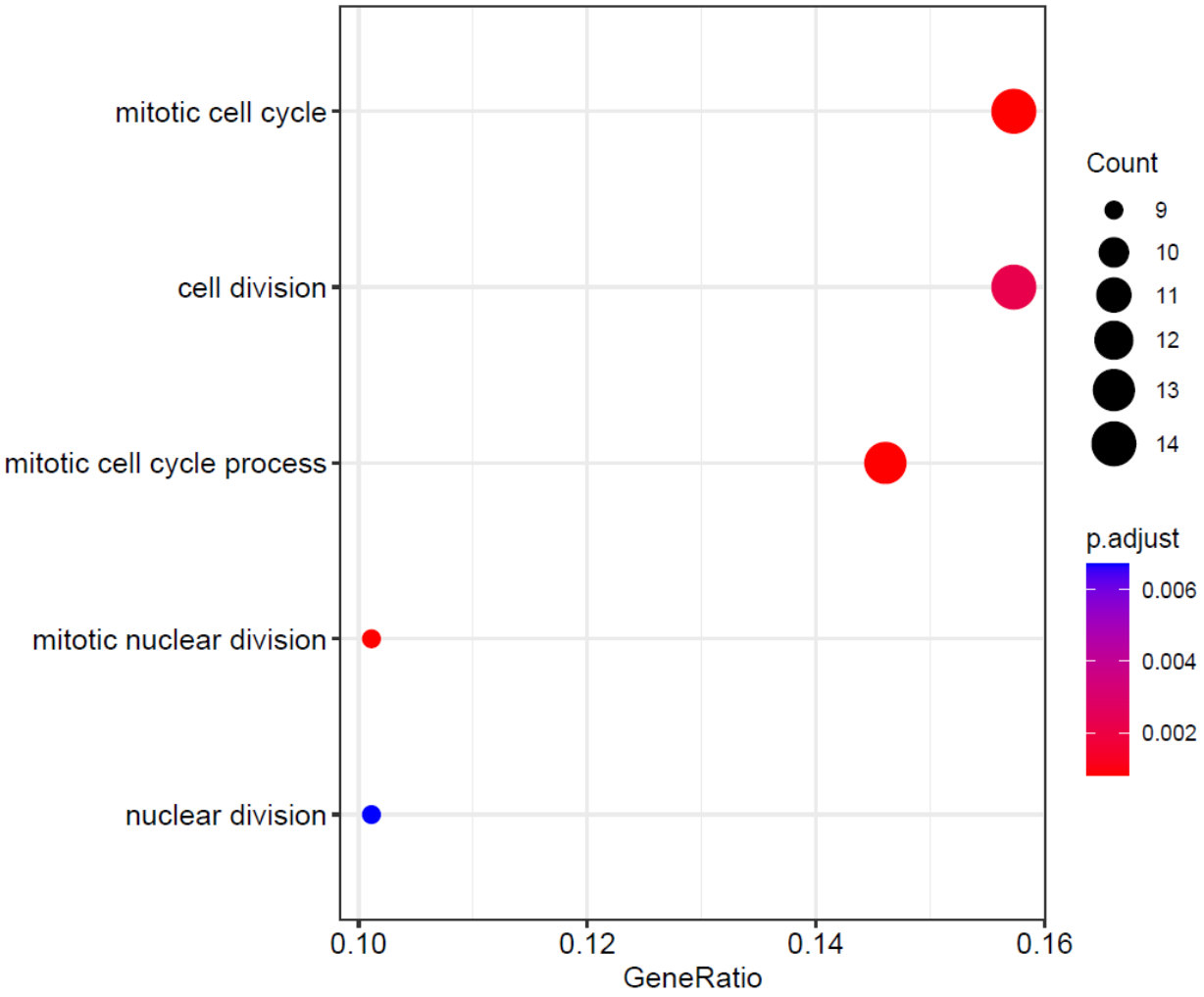

Figure 17. Page 46. GO enrichment results for annotated genes at 3 MPI. The size of the bubbles indicates the number of enriched genes in the GO analysis.

At 9 MPI (**Figure 18**), fifteen pathways were enriched. Two pathways were related to cell proliferation and thirteen pathways are involved in protein production and secretion processes. Notably, these thirteen pathways were particularly related to the membrane-vacule-endoplasmic-reticulum network which is known to be a signature feature for PrPsc propogation[1,98,116]. These findings suggest that CWD disease progression after nine months of infection includes alterations in protein trafficking.

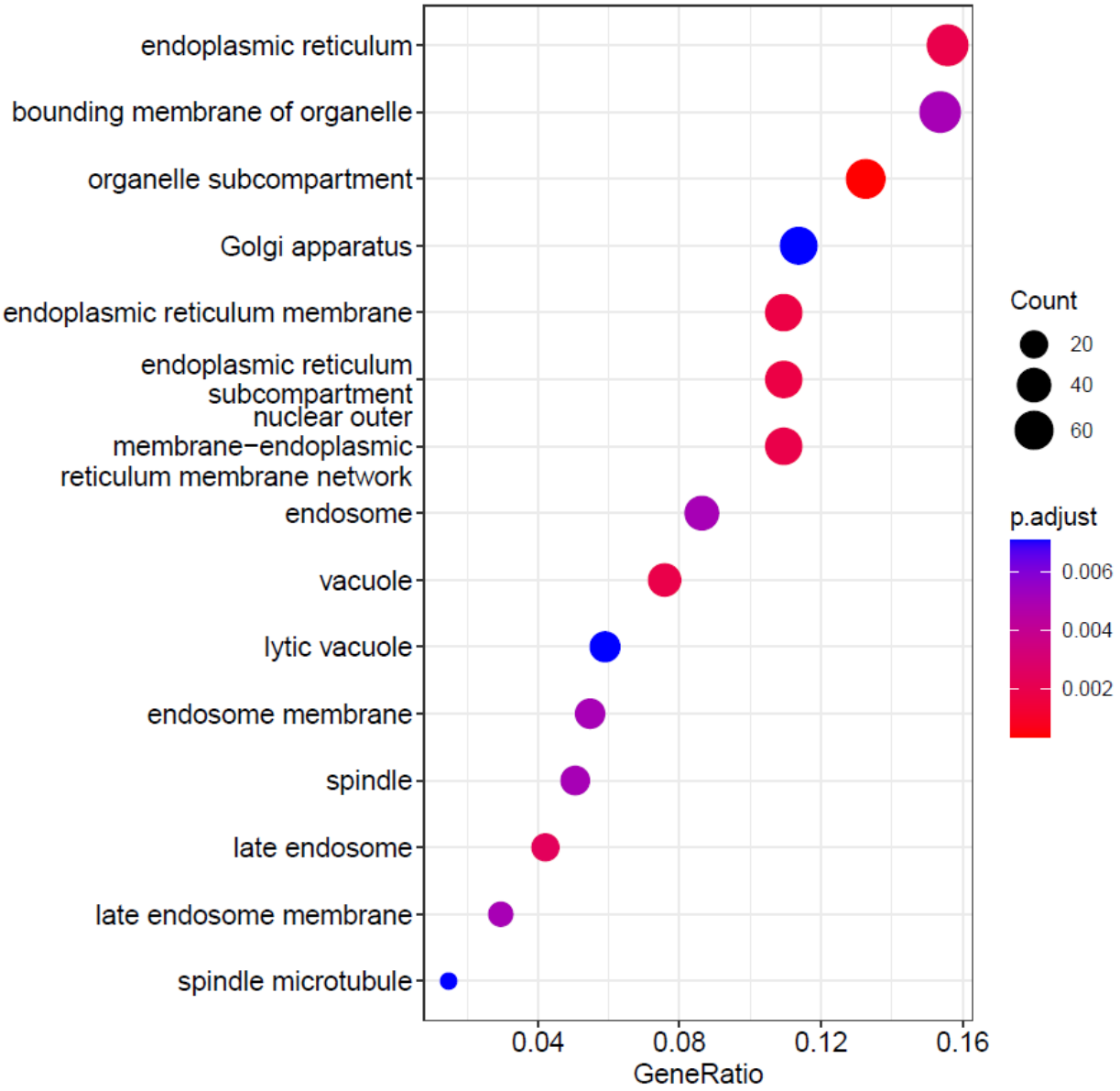

Figure 18. Page 47. GO enrichment results for annotated genes at 9 MPI. In total, fifteen pathways were enriched. Two pathways are related to cell proliferation, and thirteen pathways are related to vesicle-membrane-trafficking. The size of the bubbles indicates the count of enrichment genes in the GO analysis.

GO analysis of the DEGs identified at 12 MPI (**Figure 19**) identified fourteen enriched pathways. Of these, ten out of fourteen were embryonic and reproductive development pathways. Remarkably, four enriched pathways were related to apoptosis and autophagy progress. Autophagy was confirmed that take place in prion diseases, yet its exact role remains uncertain[61,117], but our finding provides evidence of the occurrence time of autophagy in CWD progression at 12 MPI. Apoptosis has been widely considered a primary form of programmed cell death implicated in neurodegeneration in prion diseases[61,118,119]. A sequence of evidence shows that PrPsc is involved in apoptosis which is caused by endoplasmic reticulum stress (ER stress)[61,105,120,121] and astrogliosis in the medulla oblongata and the prefrontal cortex[118,122,123], which correspond to the result of extrinsic apoptosis pathways identified at 12 MPI.

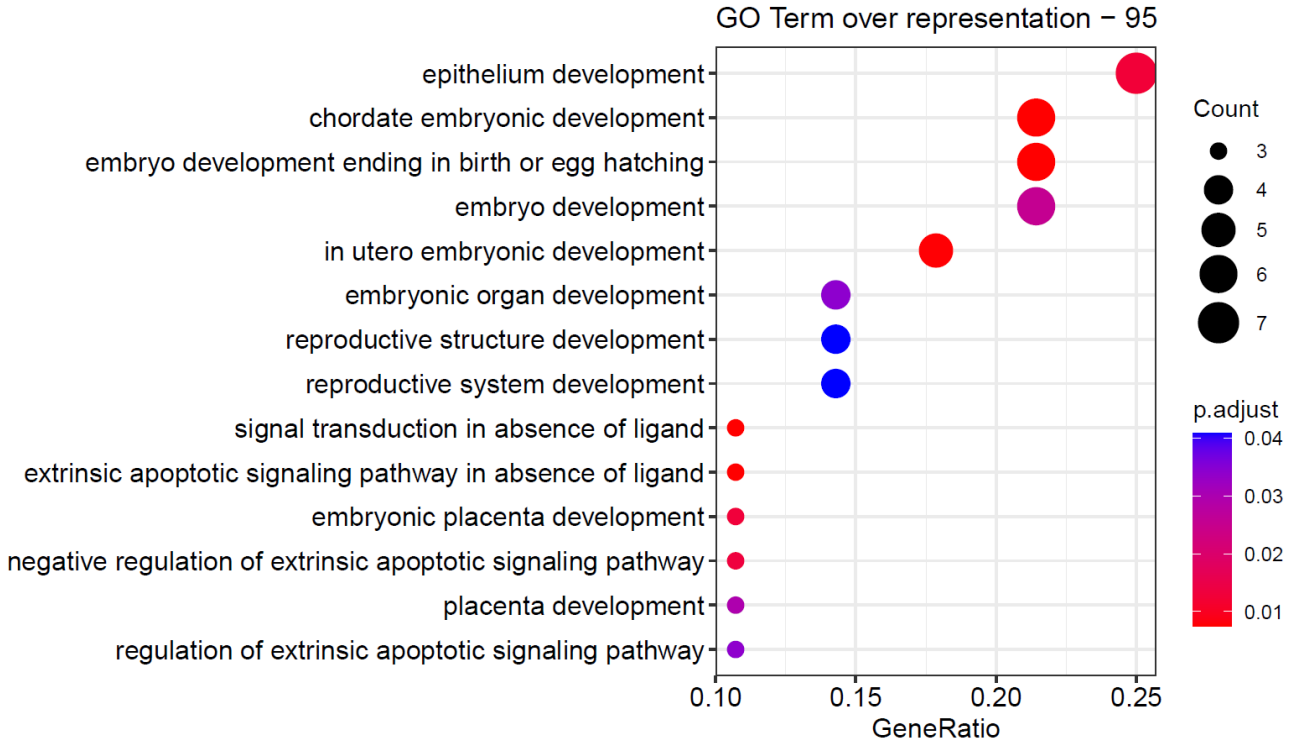

Figure 19. Page 48. GO enrichment results for annotated genes at 12 MPI. Fourteen pathways were enriched at this time point. The size of the bubbles indicates the count of enrichment genes in the GO analysis.

At 15 MPI (**Figure 20**), nine pathways were enriched, eight of which take part in protein modification processes. Notably, these eight enriched pathways suggest that protein modification was severely affected in tissues represented in the nasal swabs due to CWD infection at 15 MPI.

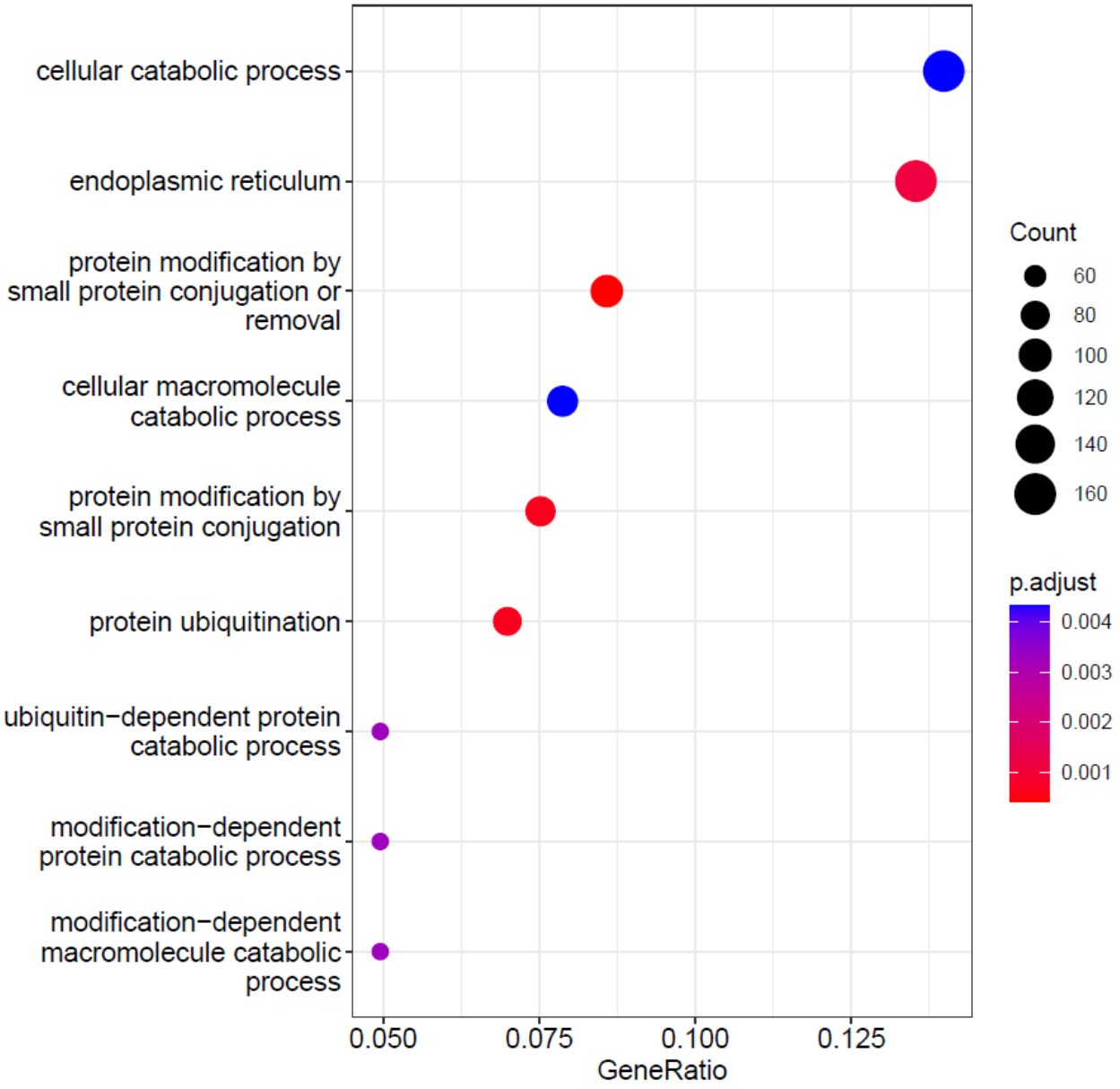

Figure 20. Page 49. GO enrichment results for annotated genes at 15 MPI. The size of the bubbles indicates the count of enrichment genes in the GO analysis.

In order to know the connection between DEGs and enriched pathways, we also did a KEGG pathway analysis. The results are shown in net plots (**Figures 21-23**).

At 3 MPI (**Figure 21**), three downregulated genes (PLK1, CDC25C, and BUB1) were clustered with all three enriched pathways: progesterone-mediated oocyte maturation pathways, oocyte meiosis pathway, and cell cycle pathway. Though these pathways have not been provided that they have a connection to prion diseases yet, PLK1 and CDC25C gene was reported to be related to the scrapie in hamster[124], CDC25C was downregulated, and PLK1 genes were identified as upregulated in CNS tissue with time[124]. PLK1 belongs to a polo-like kinases family, which controls a number of cell cycle processes, and its substrate includes CDC25C[125,126]. In our study, we identified the expression of CDC25C and PLK1 both decreased. AURKA and CDC20 were clustered with all two enriched biological processes.

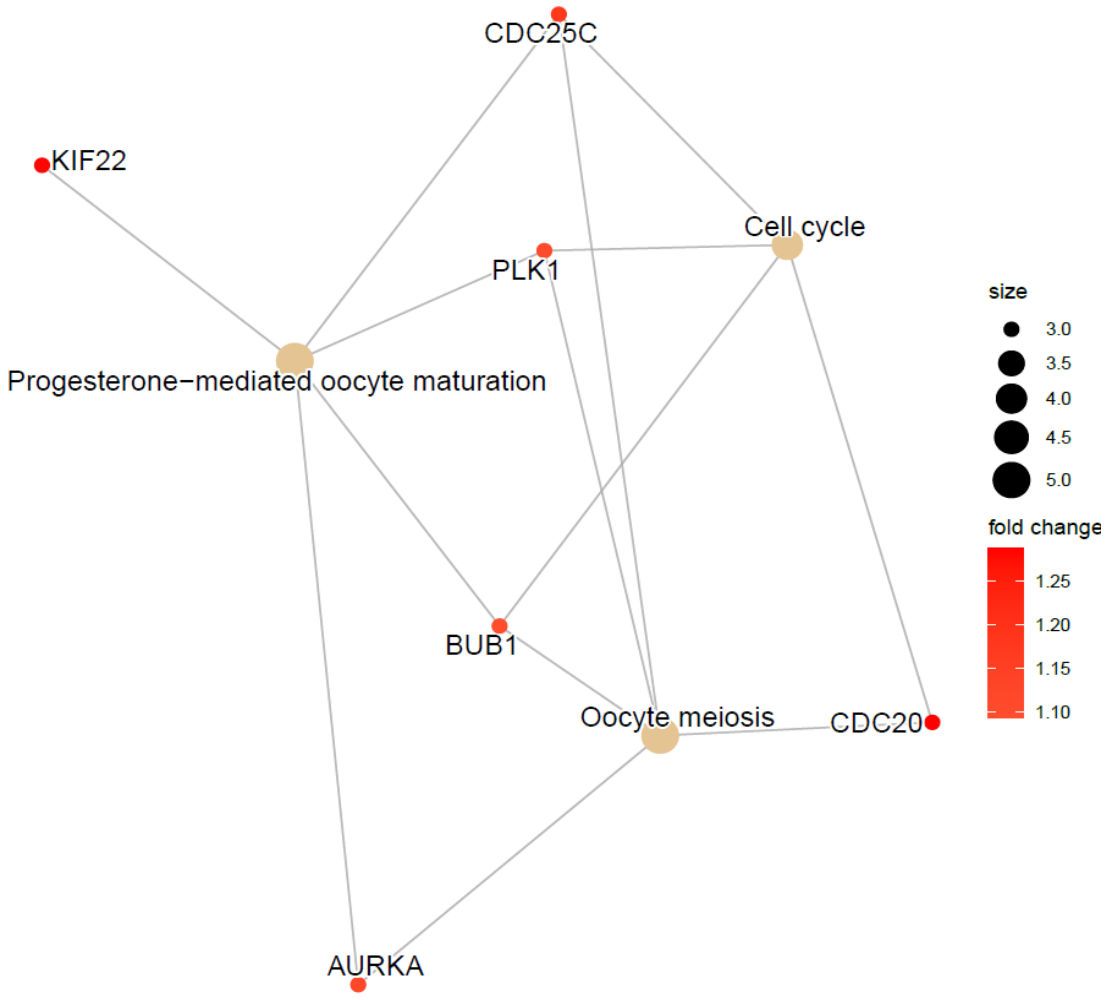

Figure 21. Page 51. KEGG analysis results of annotated genes at 3 MPI. The size of the dots indicates the number of enrichment genes for one biological process. The color bar indicated the gene`s fold change.

At 12 MPI (**Figure 22**), epithelium development pathways, nine reproduction development pathways, and four apoptosis pathways were identified. CD72, PLK4, E2F7, IFI6, HOPX, EDNRA, and COL2A1 genes were enriched to the reproduction development pathway. IFI6, COL2A1, and CD72 were enriched with apoptosis

pathways. TMOD1, CDK1, FST EDNRA, PLK4, COL2A1, and E2F7 were involved in the epithelium development pathway. Notably, COL2A1 is the only gene to have a connection to all three kinds of pathways enriched at 12 MPI, which indicates COL2A1 might have a larger contribution to CWD disease progression at 12 MPI.

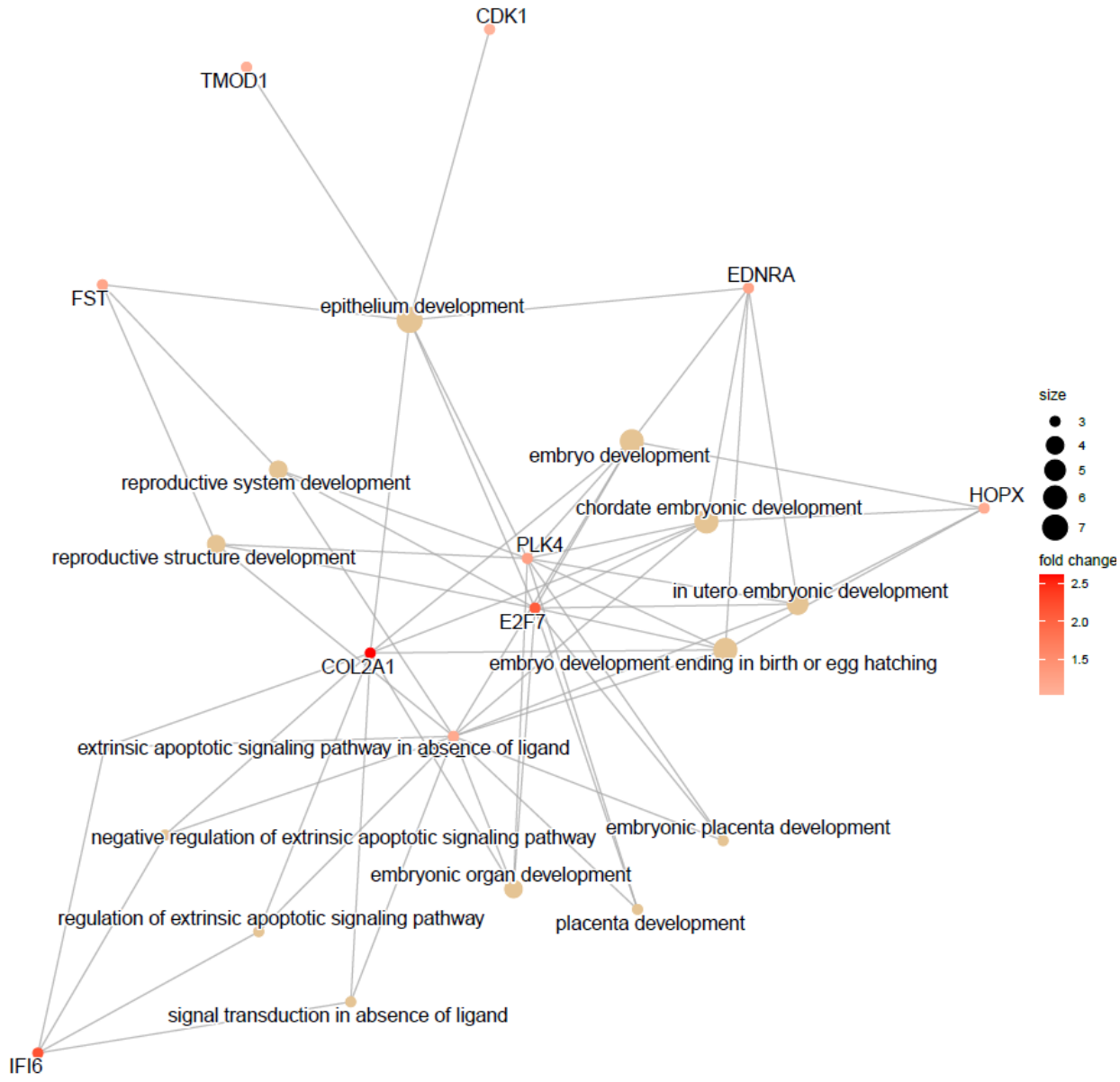

Figure 22. Page 52. KEGG analysis results of annotated genes at 12 MPI. The size of the dots indicates the number of enrichment genes for one biological process. The

color indicated the gene`s fold change; red means a bigger fold change, and pink shows a lower fold change.

At 15 MPI (**Figure 23**), eleven genes (IL10F10, TNFRSF18, IL36A, IL17RB, IL31RA, IL36RN, IL1B, CCL26, IL36G, CCR3, and CXCL14) were enriched to cytokine-cytokine receptor interactions; six genes (CLDN10, CLDN25, THY1, MYL10, CLDN17, andMYL7) were enriched to leukocyte transendothelial migration; four genes (GABRR3, GRIA3, GABRQ, and GRIN3B) were enriched to nicotine addiction. Notably, nicotine`s major binding target is nAChR, where PrPc is co-localized with the α4 subunit[127,128]. The significance of this finding is not clear because α4 subunit knock-out mice showed no difference in prion progress compared with control[128–130]. Leukocyte transendothelial migration is important for immune response, and PrPc was considered to have an effect on leukocyte recruitment[131,132]. PrPc knockout mice have a lower amount of peritoneal leukocytes responding to zymosan injected intraperitoneally[132,133].

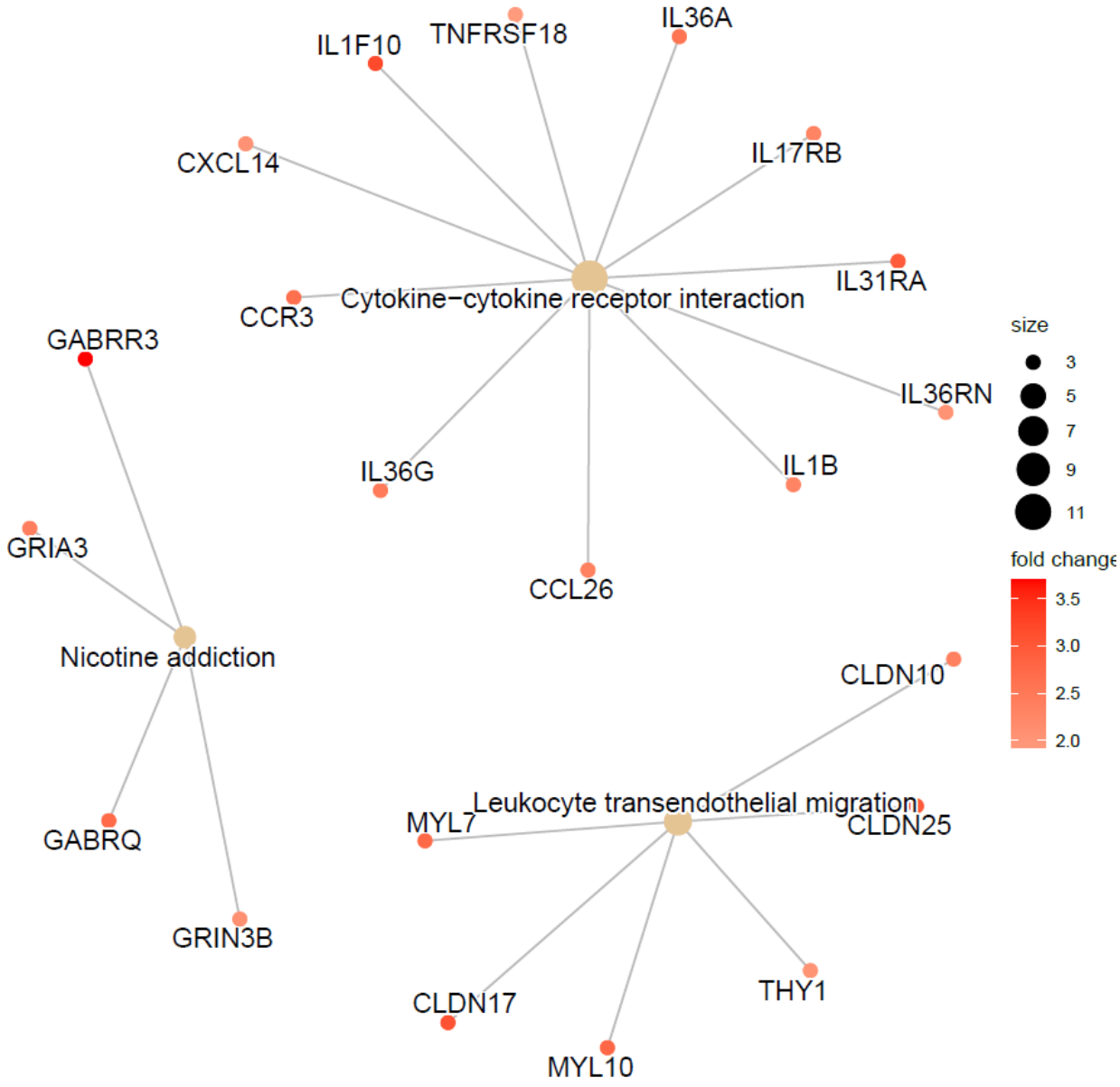

Figure 23. Page 54. KEGG analysis results of annotated genes at 15 MPI. The size of the dots indicates the number of enrichment genes for one biological process. The color indicated the gene`s fold change; red means a bigger fold change, and pink shows a lower fold change.

Conclusions

In this chapter, we performed analyses of our sequencing results of nasal swabs from CWD infected compared to control animals using GSEA with hallmark gene sets, the GO database, and the KEGG database, and we found enriched results varied with time, which might indicate CWD progressed with time and its pathogenesis and disease progression was differential at different time points.

We found that the E2F pathway, the G2M pathway, and the Mitotic spindle pathways were suppressed at all the time points examined (from 3 MPI to 15 MPI). These findings suggest that CWD may suppress cell proliferation and division progress in the nasal cavity. In previous studies, PrPc was shown to have a positive effect on cellular proliferation and differentiation of neural stem/ precursor cells in the mammalian subventricular zone[134,135], and a lack of PrPc may cause the neural cell adhesion molecule to fail to promote neuronal differentiation and induce cycling neuroblast accumulations[136]. These results suggest that there might be PrPc conformational change happening in the nasal tissues due to PrPsc seeding, which has been reported in other prion diseases[92,93].

At 3 MPI to 6 MPI, all hallmark immune-related pathways (allograft rejection, complement pathway, inflammatory response, interferon-alpha response pathway, and interferon-gamma response) were all suppressed. These findings suggest no prion shred in the nasal in the early stages of CWD infection. Starting at 9 MPI, except for the interferon-alpha response pathway and interferon-gamma response pathway, all three other enriched immune response pathways were highly activated. Because PrPsc is converted from PrPc and shown in studies, there is a lack of an anti-PrPsc antibody, which might be due to the tolerance of the immune system to PrPc, it is not likely to trigger an immune response directly[137–140]. However, these identified activated immune responses might be induced by PrPsc production and shedding in the nasal tissues. It has been shown in scrapie-infected hamsters that prions can replicate to high levels in the olfactory sensory epithelium (OSE) and induce apoptosis in olfactory receptor

neurons (ORNs)[141]. Another possible explanation of the activation of immune response pathways is they might be triggered by inflammation materials from cell apoptosis and autophagy caused by CWD infection[61]. At 12 MPI, all enriched immune response pathways mentioned above were activated, and this might suggest that with the CWD disease development, the immune response related to the CWD infection keeps progressing in the nasal tissues. The reason why 15 MPI had no enriched immune response pathway remains unclear and needs future research and explanation.

Some of the 9 MPI-enriched pathways identified were unique to this time point. These included thirteen membrane-vacule-endoplasmic-reticulum-related pathways. PrPc is a membrane protein involved in the protein-trafficking processes, and protein-trafficking dysfunction is known to be a signature feature for prion infection and other neurodegenerative diseases involving protein misfolding[1,98,116]. At 12 MPI, remarkably, four enriched pathways were related to apoptosis and autophagy progress which may be due to cell death induced by PrPsc accumulation in olfactory neurons[61,105].

At 15 MPI nine pathways were enriched, eight of which take part in protein modification processes. Notably, the misfolded PrPsc is the pathogen of prion disease, so these eight enriched pathways might indicate protein modification was severely affected due to CWD infection at 15 MPI.

Many hormone-related pathways and reproductive pathways were identified at all the time points which indicated CWD infection has an effect on hormone activity. In support of these findings, previous studies have reported alterations in hormone activity in scrapie-infected mice, scrapie-infected sheep, and humans with CJD[103,142–147].

It is possible that some of the DEGs detected may be related to seasonal differences affecting the deer. The white-tailed deer rutting season is from November to February, which is when the 9 MPI samples were collected (12/23/2020). Similarly, the effect of aging may have contributed to the DEGs identified in nasal swab samples over time. Additional studies are needed to rule these factors in/out with regard to the induction of the DEGs detected. A comparison of the 438 identified DEGs identified in this study with previous studies that identified DEGs associated with prion diseases showed that

ALOX5, FKBP5, ITGAM, SNAI2, UHRF1, CYP4F2, DDIT4, FKBP5, ITGAM, SNAI2, and UHRF1 genes were shown to be similarly altered in the brain tissue from scrapie-infected rodents, serum from CWD-infected elk, brain, liver and lymphoid nodes from CWD-infected white-tailed deer[98,106,143,148]. CDC, PLK, HSP, and GRP families of genes identified in our study also have been reported in brain tissue from scrapie-infected rodents, prion-yeast model, brain tissue and lymphoid nodes from CWD-infected white-tailed deer[106,124,149–152]. COL2A1 gene is a protein-coding gene associated with fibrillar collagen binding which is essential for cartilaginous and the normal embryonic development of the skeleton. The specific connection between COL2A1 and CWD pathogenesis has not been described before in other prion diseases.

In summary, these studies of CWD biomarkers and enriched-gene-related pathways in white-tailed deer nasal swab samples provide new insights into CWD pathogenesis and disease progression, but the specific contribution of these genes and associated pathways to CWD pathogenesis still remains unclear and needs further explanation.

References

1 Jankovska N, Rusina R, Bruzova M, Parobkova E, Olejar T, Matej R. Human Prion Disorders: Review of the Current Literature and a Twenty-Year Experience of the National Surveillance Center in the Czech Republic. *Diagnostics (Basel)* 2021;**11.**: https://doi.org/10.3390/diagnostics11101821.

2 Sikorska B, Knight R, Ironside JW, Liberski PP. Creutzfeldt-Jakob disease. *Adv Exp Med Biol* 2012;**724**:76–90. https://doi.org/10.1007/978-1-4614-0653-2_6.

3 Hill AF, Joiner S, Wadsworth JDF, Sidle KCL, Bell JE, Budka H, *et al.* Molecular classification of sporadic Creutzfeldt-Jakob disease. *Brain* 2003;**126**:1333–46. https://doi.org/10.1093/brain/awg125.

4 Collinge J. Variant Creutzfeldt-Jakob disease. *Lancet* 1999;**354**:317–23. https://doi.org/10.1016/S0140-6736(99)05128-4.

5 Creutzfeldt HG. Über eine eigenartige herdförmige erkrankung des zentralnervensystems (Vorläufige mitteilung). *Arch Psychiatr Nervenkr Z Gesamte Neurol Psychiatr* 1920;**57**:1–18. https://doi.org/10.1007/bf02866081.

6 Henry R, Murphy F. Etymologia: Creutzfeldt-Jakob Disease. *Emerging Infectious Disease Journal* 2017;**23**:956. https://doi.org/10.3201/eid2306.et2306.

7 Baker HF, Ridley RM. *Prion Diseases*. Humana Press; 1996.

8 Hilton DA. Pathogenesis and prevalence of variant Creutzfeldt-Jakob disease. *J Pathol* 2006;**208**:134–41. https://doi.org/10.1002/path.1880.

9 Brown P, Cathala F, Raubertas RF, Gajdusek DC, Castaigne P. The epidemiology of Creutzfeldt-Jakob disease: conclusion of a 15-year investigation in France and review of the world literature. *Neurology* 1987;**37**:895–904. https://doi.org/10.1212/wnl.37.6.895.

10 Uttley L, Carroll C, Wong R, Hilton DA, Stevenson M. Creutzfeldt-Jakob disease: a systematic review of global incidence, prevalence, infectivity, and incubation. *Lancet Infect Dis* 2020;**20**:e2–10. https://doi.org/10.1016/S1473-3099(19)30615-2.

11 Gao L-P, Shi Q, Xiao K, Wang J, Zhou W, Chen C, *et al.* The genetic Creutzfeldt-Jakob disease with E200K mutation: analysis of clinical, genetic and laboratory features of 30 Chinese patients. *Sci Rep* 2019;**9**:1836. https://doi.org/10.1038/s41598-019-38520-y.

12 Will RG. Acquired prion disease: iatrogenic CJD, variant CJD, kuru. *Br Med Bull* 2003;**66**:255–65. https://doi.org/10.1093/bmb/66.1.255.

13 Gajdusek DC, Zigas V. Degenerative disease of the central nervous system in New Guinea; the endemic occurrence of kuru in the native population. *N Engl J Med* 1957;**257**:974–8. https://doi.org/10.1056/NEJM195711142572005.

14 Alpers MP. A history of kuru. *P N G Med J* 2007;**50**:10–9.

15 Medori R, Montagna P, Tritschler HJ, LeBlanc A, Cortelli P, Tinuper P, *et al.* Fatal familial insomnia: a second kindred with mutation of prion protein gene at codon 178. *Neurology* 1992;**42**:669–70. https://doi.org/10.1212/wnl.42.3.669.

16 Lugaresi E, Medori R, Montagna P, Baruzzi A, Cortelli P, Lugaresi A, *et al.* Fatal familial insomnia and dysautonomia with selective degeneration of thalamic nuclei. *N Engl J Med* 1986;**315**:997–1003.

https://doi.org/10.1056/NEJM198610163151605.
17 Liberski PP. Gerstmann-Sträussler-Scheinker Disease. In: Ahmad SI, editor. *Neurodegenerative Diseases*. New York, NY: Springer US; 2012. p. 128–37.
18 Ghetti B, Dlouhy SR, Giaccone G, Bugiani O, Frangione B, Farlow MR, *et al.* Gerstmann-Sträussler-Scheinker disease and the Indiana kindred. *Brain Pathol* 1995;**5**:61–75. https://doi.org/10.1111/j.1750-3639.1995.tb00578.x.
19 Nathanson N, Wilesmith J, Griot C. Bovine spongiform encephalopathy (BSE): causes and consequences of a common source epidemic. *Am J Epidemiol* 1997;**145**:959–69. https://doi.org/10.1093/oxfordjournals.aje.a009064.
20 Nunnally BK, Krull IS. *Prions and Mad Cow Disease*. Taylor & Francis; 2003.
21 Smith PG, Bradley R. Bovine spongiform encephalopathy (BSE) and its epidemiology. *Br Med Bull* 2003;**66**:185–98. https://doi.org/10.1093/bmb/66.1.185.
22 Griffith JS. Nature of the Scrapie Agent: Self-replication and Scrapie. *Nature* 1967;**215**:1043–4. https://doi.org/10.1038/2151043a0.
23 Detwiler LA, Baylis M. The epidemiology of scrapie. *Rev Sci Tech* 2003;**22**:121–43. https://doi.org/10.20506/rst.22.1.1386.
24 Foster JD, Parnham D, Chong A, Goldmann W, Hunter N. Clinical signs, histopathology and genetics of experimental transmission of BSE and natural scrapie to sheep and goats. *Vet Rec* 2001;**148**:165–71. https://doi.org/10.1136/vr.148.6.165.
25 Marsh RF, Hadlow WJ. Transmissible mink encephalopathy. *Rev Sci Tech* 1992;**11**:539–50. https://doi.org/10.20506/rst.11.2.606.
26 Bessen RA, Marsh RF. Biochemical and physical properties of the prion protein from two strains of the transmissible mink encephalopathy agent. *J Virol* 1992;**66**:2096–101. https://doi.org/10.1128/JVI.66.4.2096-2101.1992.
27 Bessen RA, Marsh RF. Distinct PrP properties suggest the molecular basis of strain variation in transmissible mink encephalopathy. *J Virol* 1994;**68**:7859–68. https://doi.org/10.1128/JVI.68.12.7859-7868.1994.
28 Bessen RA, Kocisko DA, Raymond GJ, Nandan S, Lansbury PT, Caughey B. Non-genetic propagation of strain-specific properties of scrapie prion protein. *Nature* 1995;**375**:698–700. https://doi.org/10.1038/375698a0.
29 Haley NJ, Richt JA. Evolution of Diagnostic Tests for Chronic Wasting Disease, a Naturally Occurring Prion Disease of Cervids. *Pathogens* 2017;**6.**: https://doi.org/10.3390/pathogens6030035.
30 Williams ES, Miller MW. Chronic wasting disease in deer and elk in North America. *Rev Sci Tech* 2002;**21**:305–16. https://doi.org/10.20506/rst.21.2.1340.
31 *Occurrence*. 2023. URL: https://www.cdc.gov/prions/cwd/occurrence.html (Accessed 2 August 2023).
32 Benvegnù S, Poggiolini I, Legname G. Neurodevelopmental expression and localization of the cellular prion protein in the central nervous system of the mouse. *J Comp Neurol* 2010;**518**:1879–91. https://doi.org/10.1002/cne.22357.
33 Stahl N, Borchelt DR, Hsiao K, Prusiner SB. Scrapie prion protein contains a phosphatidylinositol glycolipid. *Cell* 1987;**51**:229–40. https://doi.org/10.1016/0092-8674(87)90150-4.
34 Viles JH, Cohen FE, Prusiner SB, Goodin DB, Wright PE, Dyson HJ. Copper

binding to the prion protein: structural implications of four identical cooperative binding sites. *Proc Natl Acad Sci U S A* 1999;**96**:2042–7. https://doi.org/10.1073/pnas.96.5.2042.
35 Jackson GS, Murray I, Hosszu LL, Gibbs N, Waltho JP, Clarke AR, *et al.* Location and properties of metal-binding sites on the human prion protein. *Proc Natl Acad Sci U S A* 2001;**98**:8531–5. https://doi.org/10.1073/pnas.151038498.
36 Kurschner C, Morgan JI. The cellular prion protein (PrP) selectively binds to Bcl-2 in the yeast two-hybrid system. *Brain Res Mol Brain Res* 1995;**30**:165–8. https://doi.org/10.1016/0169-328x(95)00013-i.
37 Kuwahara C, Takeuchi AM, Nishimura T, Haraguchi K, Kubosaki A, Matsumoto Y, *et al.* Prions prevent neuronal cell-line death. *Nature* 1999;**400**:225–6. https://doi.org/10.1038/22241.
38 Herms J, Tings T, Gall S, Madlung A, Giese A, Siebert H, *et al.* Evidence of presynaptic location and function of the prion protein. *J Neurosci* 1999;**19**:8866–75. https://doi.org/10.1523/JNEUROSCI.19-20-08866.1999.
39 Spielhaupter C, Schätzl HM. PrPC directly interacts with proteins involved in signaling pathways. *J Biol Chem* 2001;**276**:44604–12. https://doi.org/10.1074/jbc.M103289200.
40 Lledo PM, Tremblay P, DeArmond SJ, Prusiner SB, Nicoll RA. Mice deficient for prion protein exhibit normal neuronal excitability and synaptic transmission in the hippocampus. *Proc Natl Acad Sci U S A* 1996;**93**:2403–7. https://doi.org/10.1073/pnas.93.6.2403.
41 Sanz-Hernández M, Barritt JD, Sobek J, Hornemann S, Aguzzi A, De Simone A. Mechanism of misfolding of the human prion protein revealed by a pathological mutation. *Proc Natl Acad Sci U S A* 2021;**118.**: https://doi.org/10.1073/pnas.2019631118.
42 Prusiner SB, Groth DF, Bolton DC, Kent SB, Hood LE. Purification and structural studies of a major scrapie prion protein. *Cell* 1984;**38**:127–34. https://doi.org/10.1016/0092-8674(84)90533-6.
43 Novakofski J, Brewer MS, Mateus-Pinilla N, Killefer J, McCusker RH. Prion biology relevant to bovine spongiform encephalopathy. *J Anim Sci* 2005;**83**:1455–76. https://doi.org/10.2527/2005.8361455x.
44 Prusiner SB, Groth D, Serban A, Koehler R, Foster D, Torchia M, *et al.* Ablation of the prion protein (PrP) gene in mice prevents scrapie and facilitates production of anti-PrP antibodies. *Proc Natl Acad Sci U S A* 1993;**90**:10608–12. https://doi.org/10.1073/pnas.90.22.10608.
45 Brandner S, Raeber A, Sailer A, Blättler T, Fischer M, Weissmann C, *et al.* Normal host prion protein (PrP^C) is required for scrapie spread within the central nervous system. *Proc Natl Acad Sci U S A* 1996;**93**:13148–51. https://doi.org/10.1073/pnas.93.23.13148.
46 Goldmann W, Martin T, Foster J, Hughes S, Smith G, Hughes K, *et al.* Novel polymorphisms in the caprine PrP gene: a codon 142 mutation associated with scrapie incubation period. *J Gen Virol* 1996;**77 (Pt 11)**:2885–91. https://doi.org/10.1099/0022-1317-77-11-2885.
47 Goldmann W, Hunter N, Foster JD, Salbaum JM, Beyreuther K, Hope J. Two

alleles of a neural protein gene linked to scrapie in sheep. *Proc Natl Acad Sci U S A* 1990;**87**:2476–80. https://doi.org/10.1073/pnas.87.7.2476.
48 Kretzschmar HA, Prusiner SB, Stowring LE, DeArmond SJ. Scrapie prion proteins are synthesized in neurons. *Am J Pathol* 1986;**122**:1–5.
49 Puckett C, Concannon P, Casey C, Hood L. Genomic structure of the human prion protein gene. *Am J Hum Genet* 1991;**49**:320–9.
50 Lee IY, Westaway D, Smit AF, Wang K, Seto J, Chen L, *et al.* Complete genomic sequence and analysis of the prion protein gene region from three mammalian species. *Genome Res* 1998;**8**:1022–37. https://doi.org/10.1101/gr.8.10.1022.
51 Hornshaw MP, McDermott JR, Candy JM. Copper binding to the N-terminal tandem repeat regions of mammalian and avian prion protein. *Biochem Biophys Res Commun* 1995;**207**:621–9. https://doi.org/10.1006/bbrc.1995.1233.
52 Haynes MP, Sinha D, Russell KS, Collinge M, Fulton D, Morales-Ruiz M, *et al.* Membrane Estrogen Receptor Engagement Activates Endothelial Nitric Oxide Synthase via the PI3-Kinase–Akt Pathway in Human Endothelial Cells. *Circ Res* 2000;**87**:677–82. https://doi.org/10.1161/01.RES.87.8.677.
53 Wüthrich K, Riek R. Three-dimensional structures of prion proteins. *Adv Protein Chem* 2001;**57**:55–82. https://doi.org/10.1016/s0065-3233(01)57018-7.
54 Riek R, Hornemann S, Wider G, Glockshuber R, Wüthrich K. NMR characterization of the full-length recombinant murine prion protein, mPrP(23–231). *FEBS Lett* 1997;**413**:282–8. https://doi.org/10.1016/S0014-5793(97)00920-4.
55 Riesner D. Biochemistry and structure of PrPC and PrPSc. *Br Med Bull* 2003;**66**:21–33. https://doi.org/10.1093/bmb/66.1.21.
56 Pan KM, Baldwin M, Nguyen J, Gasset M, Serban A, Groth D, *et al.* Conversion of alpha-helices into beta-sheets features in the formation of the scrapie prion proteins. *Proc Natl Acad Sci U S A* 1993;**90**:10962–6. https://doi.org/10.1073/pnas.90.23.10962.
57 Sulkowski E. Spontaneous conversion of PrPC to PrPSc. *FEBS Lett* 1992;**307**:129–30. https://doi.org/10.1016/0014-5793(92)80750-b.
58 Eghiaian F, Grosclaude J, Lesceu S, Debey P, Doublet B, Tréguer E, *et al.* Insight into the $PrP^{C} \rightarrow PrP^{Sc}$ conversion from the structures of antibody-bound ovine prion scrapie-susceptibility variants. *Proceedings of the National Academy of Sciences* 2004;**101**:10254–9. https://doi.org/10.1073/pnas.0400014101.
59 Selvaggini C, De Gioia L, Cantù L, Ghibaudi E, Diomede L, Passerini F, *et al.* Molecular characteristics of a protease-resistant, amyloidogenic and neurotoxic peptide homologous to residues 106-126 of the prion protein. *Biochem Biophys Res Commun* 1993;**194**:1380–6. https://doi.org/10.1006/bbrc.1993.1977.
60 McKinley MP, Bolton DC, Prusiner SB. A protease-resistant protein is a structural component of the scrapie prion. *Cell* 1983;**35**:57–62. https://doi.org/10.1016/0092-8674(83)90207-6.
61 Liberski PP, Sikorska B, Bratosiewicz-Wasik J, Gajdusek DC, Brown P. Neuronal cell death in transmissible spongiform encephalopathies (prion diseases) revisited: from apoptosis to autophagy. *Int J Biochem Cell Biol* 2004;**36**:2473–90. https://doi.org/10.1016/j.biocel.2004.04.016.
62 Moore SJ, Kunkle R, Greenlee MHW, Nicholson E, Richt J, Hamir A, *et al.*

Horizontal Transmission of Chronic Wasting Disease in Reindeer. *Emerg Infect Dis* 2016;**22**:2142–5. https://doi.org/10.3201/eid2212.160635.
63 Miller MW, Williams ES. Horizontal prion transmission in mule deer. *Nature* 2003;**425**:35–6. https://doi.org/10.1038/425035a.
64 Plummer IH, Wright SD, Johnson CJ, Pedersen JA, Samuel MD. Temporal patterns of chronic wasting disease prion excretion in three cervid species. *J Gen Virol* 2017;**98**:1932–42. https://doi.org/10.1099/jgv.0.000845.
65 Woolhouse ME, Matthews L, Coen P, Stringer SM, Foster JD, Hunter N. Population dynamics of scrapie in a sheep flock. *Philos Trans R Soc Lond B Biol Sci* 1999;**354**:751–6. https://doi.org/10.1098/rstb.1999.0427.
66 Mabbott NA. How do PrPSc Prions Spread between Host Species, and within Hosts? *Pathogens* 2017;**6.**: https://doi.org/10.3390/pathogens6040060.
67 Gough KC, Baker CA, Rees HC, Terry LA, Spiropoulos J, Thorne L, *et al.* The oral secretion of infectious scrapie prions occurs in preclinical sheep with a range of PRNP genotypes. *J Virol* 2012;**86**:566–71. https://doi.org/10.1128/JVI.05579-11.
68 Hase K, Kawano K, Nochi T, Pontes GS, Fukuda S, Ebisawa M, *et al.* Uptake through glycoprotein 2 of FimH+ bacteria by M cells initiates mucosal immune response. *Nature* 2009;**462**:226–30. https://doi.org/10.1038/nature08529.
69 Mabbott NA, Bradford BM, Pal R, Young R, Donaldson DS. The Effects of Immune System Modulation on Prion Disease Susceptibility and Pathogenesis. *Int J Mol Sci* 2020;**21.**: https://doi.org/10.3390/ijms21197299.
70 Kujala P, Raymond CR, Romeijn M, Godsave SF, van Kasteren SI, Wille H, *et al.* Prion uptake in the gut: identification of the first uptake and replication sites. *PLoS Pathog* 2011;**7**:e1002449. https://doi.org/10.1371/journal.ppat.1002449.
71 Kitamoto T, Muramoto T, Mohri S, Doh-Ura K, Tateishi J. Abnormal isoform of prion protein accumulates in follicular dendritic cells in mice with Creutzfeldt-Jakob disease. *J Virol* 1991;**65**:6292–5. https://doi.org/10.1128/JVI.65.11.6292-6295.1991.
72 Glatzel M, Heppner FL, Albers KM, Aguzzi A. Sympathetic innervation of lymphoreticular organs is rate limiting for prion neuroinvasion. *Neuron* 2001;**31**:25–34. https://doi.org/10.1016/s0896-6273(01)00331-2.
73 McBride PA, Schulz-Schaeffer WJ, Donaldson M, Bruce M, Diringer H, Kretzschmar HA, *et al.* Early spread of scrapie from the gastrointestinal tract to the central nervous system involves autonomic fibers of the splanchnic and vagus nerves. *J Virol* 2001;**75**:9320–7. https://doi.org/10.1128/JVI.75.19.9320-9327.2001.
74 Prinz M, Heikenwalder M, Junt T, Schwarz P, Glatzel M, Heppner FL, *et al.* Positioning of follicular dendritic cells within the spleen controls prion neuroinvasion. *Nature* 2003;**425**:957–62. https://doi.org/10.1038/nature02072.
75 Puoti G, Bizzi A, Forloni G, Safar JG, Tagliavini F, Gambetti P. Sporadic human prion diseases: molecular insights and diagnosis. *Lancet Neurol* 2012;**11**:618–28. https://doi.org/10.1016/S1474-4422(12)70063-7.
76 Geschwind MD. Prion Diseases. *Continuum* 2015;**21**:1612–38. https://doi.org/10.1212/CON.0000000000000251.
77 Aguzzi A, Heikenwalder M, Miele G. Progress and problems in the biology, diagnostics, and therapeutics of prion diseases. *J Clin Invest* 2004;**114**:153–60.

https://doi.org/10.1172/JCI22438.
78 Wells GA, Hawkins SA, Green RB, Austin AR, Dexter I, Spencer YI, *et al.* Preliminary observations on the pathogenesis of experimental bovine spongiform encephalopathy (BSE): an update. *Vet Rec* 1998;**142**:103–6. https://doi.org/10.1136/vr.142.5.103.
79 Herbst A, Wohlgemuth S, Yang J, Castle AR, Moreno DM, Otero A, *et al.* Susceptibility of Beavers to Chronic Wasting Disease. *Biology* 2022;**11.**: https://doi.org/10.3390/biology11050667.
80 Heisey DM, Mickelsen NA, Schneider JR, Johnson CJ, Johnson CJ, Langenberg JA, *et al.* Chronic wasting disease (CWD) susceptibility of several North American rodents that are sympatric with cervid CWD epidemics. *J Virol* 2010;**84**:210–5. https://doi.org/10.1128/JVI.00560-09.
81 Castilla J, Gonzalez-Romero D, Saá P, Morales R, De Castro J, Soto C. Crossing the species barrier by PrP(Sc) replication in vitro generates unique infectious prions. *Cell* 2008;**134**:757–68. https://doi.org/10.1016/j.cell.2008.07.030.
82 Collinge J. Medicine. Prion strain mutation and selection. *Science* 2010:1111–2. https://doi.org/10.1126/science.1190815.
83 Béringue V, Vilotte J-L, Laude H. Prion agent diversity and species barrier. *Vet Res* 2008;**39**:47. https://doi.org/10.1051/vetres:2008024.
84 EFSA Panel on Biological Hazards (BIOHAZ), Ricci A, Allende A, Bolton D, Chemaly M, Davies R, *et al.* Chronic wasting disease (CWD) in cervids. *EFSA J* 2017;**15**:e04667. https://doi.org/10.2903/j.efsa.2017.4667.
85 Williams ES, Miller MW, Kreeger TJ, Kahn RH, Thorne ET. Chronic Wasting Disease of Deer and Elk: A Review with Recommendations for Management. *J Wildl Manage* 2002;**66**:551–63. https://doi.org/10.2307/3803123.
86 Kraft CN, Denkers ND, Mathiason CK, Hoover EA. Longitudinal detection of prion shedding in nasal secretions of CWD-infected white-tailed deer. *J Gen Virol* 2023;**104.**: https://doi.org/10.1099/jgv.0.001825.
87 Haley NJ, Siepker C, Hoon-Hanks LL, Mitchell G, Walter WD, Manca M, *et al.* Seeded Amplification of Chronic Wasting Disease Prions in Nasal Brushings and Recto-anal Mucosa-Associated Lymphoid Tissues from Elk by Real-Time Quaking-Induced Conversion. *J Clin Microbiol* 2016;**54**:1117–26. https://doi.org/10.1128/JCM.02700-15.
88 Sigurdson CJ, Barillas-Mury C, Miller MW, Oesch B, van Keulen LJM, Langeveld JPM, *et al.* PrP(CWD) lymphoid cell targets in early and advanced chronic wasting disease of mule deer. *J Gen Virol* 2002;**83**:2617–28. https://doi.org/10.1099/0022-1317-83-10-2617.
89 Sigurdson CJ, Williams ES, Miller MW, Spraker TR, O'Rourke KI, Hoover EA. Oral transmission and early lymphoid tropism of chronic wasting disease PrPres in mule deer fawns (Odocoileus hemionus). *J Gen Virol* 1999;**80 (Pt 10)**:2757–64. https://doi.org/10.1099/0022-1317-80-10-2757.
90 Balkema-Buschmann A, Eiden M, Hoffmann C, Kaatz M, Ziegler U, Keller M, *et al.* BSE infectivity in the absence of detectable PrP(Sc) accumulation in the tongue and nasal mucosa of terminally diseased cattle. *J Gen Virol* 2011;**92**:467–76. https://doi.org/10.1099/vir.0.025387-0.

91 Walter BA, Valera VA, Takahashi S, Ushiki T. The olfactory route for cerebrospinal fluid drainage into the peripheral lymphatic system. *Neuropathol Appl Neurobiol* 2006;**32**:388–96. https://doi.org/10.1111/j.1365-2990.2006.00737.x.
92 Corona C, Porcario C, Martucci F, Iulini B, Manea B, Gallo M, *et al.* Olfactory system involvement in natural scrapie disease. *J Virol* 2009;**83**:3657–67. https://doi.org/10.1128/JVI.01966-08.
93 Redaelli V, Bistaffa E, Zanusso G, Salzano G, Sacchetto L, Rossi M, *et al.* Detection of prion seeding activity in the olfactory mucosa of patients with Fatal Familial Insomnia. *Sci Rep* 2017;**7**:46269. https://doi.org/10.1038/srep46269.
94 Bessen RA, Shearin H, Martinka S, Boharski R, Lowe D, Wilham JM, *et al.* Prion shedding from olfactory neurons into nasal secretions. *PLoS Pathog* 2010;**6**:e1000837. https://doi.org/10.1371/journal.ppat.1000837.
95 Wang J, Davidson JL, Kaur S, Dextre AA, Ranjbaran M, Kamel MS, *et al.* Paper-Based Biosensors for the Detection of Nucleic Acids from Pathogens. *Biosensors* 2022;**12.**: https://doi.org/10.3390/bios12121094.
96 Sajid M, Kawde A-N, Daud M. Designs, formats and applications of lateral flow assay: A literature review. *Journal of Saudi Chemical Society* 2015;**19**:689–705. https://doi.org/10.1016/j.jscs.2014.09.001.
97 Islam MM, Koirala D. Toward a next-generation diagnostic tool: A review on emerging isothermal nucleic acid amplification techniques for the detection of SARS-CoV-2 and other infectious viruses. *Anal Chim Acta* 2022;**1209**:339338. https://doi.org/10.1016/j.aca.2021.339338.
98 Slota JA, Medina SJ, Klassen M, Gorski D, Mesa CM, Robertson C, *et al.* Identification of circulating microRNA signatures as potential biomarkers in the serum of elk infected with chronic wasting disease. *Sci Rep* 2019;**9**:19705. https://doi.org/10.1038/s41598-019-56249-6.
99 Jaunmuktane Z, Brandner S. Invited Review: The role of prion-like mechanisms in neurodegenerative diseases. *Neuropathol Appl Neurobiol* 2020;**46**:522–45. https://doi.org/10.1111/nan.12592.
100 Chandler RL. Experimental Scrapie in the Mouse. *Res Vet Sci* 1963;**4**:276–85. https://doi.org/10.1016/S0034-5288(18)34870-7.
101 Kimberlin RH, Walker CA. Evidence that the transmission of one source of scrapie agent to hamsters involves separation of agent strains from a mixture. *J Gen Virol* 1978;**39**:487–96. https://doi.org/10.1099/0022-1317-39-3-487.
102 Skinner PJ, Kim HO, Bryant D, Kinzel NJ, Reilly C, Priola SA, *et al.* Treatment of Prion Disease with Heterologous Prion Proteins. *PLoS One* 2015;**10**:e0131993. https://doi.org/10.1371/journal.pone.0131993.
103 Skinner P. Prion disease induced alterations in gene expression in spleen and brain prior to clinical symptoms. *Advances and Applications in Bioinformatics and Chemistry* 2008:29. https://doi.org/10.2147/aabc.s3411.
104 Hwang D, Lee IY, Yoo H, Gehlenborg N, Cho J-H, Petritis B, *et al.* A systems approach to prion disease. *Mol Syst Biol* 2009;**5**:252. https://doi.org/10.1038/msb.2009.10.
105 Basu U, Almeida LM, Dudas S, Graham CE, Czub S, Moore SS, *et al.* Gene expression alterations in Rocky Mountain elk infected with chronic wasting disease.

Prion 2012;**6**:282–301. https://doi.org/10.4161/pri.19915.
106 Trone-Launer EK, Wang J, Lu G, Mateus-Pinilla NE, Zick PR, Lamer JT, *et al.* Differential gene expression in chronic wasting disease-positive white-tailed deer (Odocoileus virginianus). *Ecol Evol* 2019;**9**:12600–12.
107 Bao R, Huang L, Andrade J, Tan W, Kibbe WA, Jiang H, *et al.* Review of current methods, applications, and data management for the bioinformatics analysis of whole exome sequencing. *Cancer Inform* 2014;**13**:67–82. https://doi.org/10.4137/CIN.S13779.
108 Fjukstad B, Bongo LA. A Review of Scalable Bioinformatics Pipelines. *Data Science and Engineering* 2017;**2**:245–51. https://doi.org/10.1007/s41019-017-0047-z.
109 Hurd PJ, Nelson CJ. Advantages of next-generation sequencing versus the microarray in epigenetic research. *Brief Funct Genomic Proteomic* 2009;**8**:174–83. https://doi.org/10.1093/bfgp/elp013.
110 Subramanian A, Tamayo P, Mootha VK, Mukherjee S, Ebert BL, Gillette MA, *et al.* Gene set enrichment analysis: a knowledge-based approach for interpreting genome-wide expression profiles. *Proc Natl Acad Sci U S A* 2005;**102**:15545–50. https://doi.org/10.1073/pnas.0506580102.
111 Mootha VK, Lindgren CM, Eriksson K-F, Subramanian A, Sihag S, Lehar J, *et al.* PGC-1alpha-responsive genes involved in oxidative phosphorylation are coordinately downregulated in human diabetes. *Nat Genet* 2003;**34**:267–73. https://doi.org/10.1038/ng1180.
112 Liberzon A, Birger C, Thorvaldsdóttir H, Ghandi M, Mesirov JP, Tamayo P. The Molecular Signatures Database (MSigDB) hallmark gene set collection. *Cell Syst* 2015;**1**:417–25. https://doi.org/10.1016/j.cels.2015.12.004.
113 Ashburner M, Ball CA, Blake JA, Botstein D, Butler H, Cherry JM, *et al.* Gene ontology: tool for the unification of biology. The Gene Ontology Consortium. *Nat Genet* 2000;**25**:25–9. https://doi.org/10.1038/75556.
114 Gene Ontology Consortium, Aleksander SA, Balhoff J, Carbon S, Cherry JM, Drabkin HJ, *et al.* The Gene Ontology knowledgebase in 2023. *Genetics* 2023;**224.**: https://doi.org/10.1093/genetics/iyad031.
115 Kanehisa M, Goto S. KEGG: kyoto encyclopedia of genes and genomes. *Nucleic Acids Res* 2000;**28**:27–30. https://doi.org/10.1093/nar/28.1.27.
116 Uchiyama K, Muramatsu N, Yano M, Usui T, Miyata H, Sakaguchi S. Prions disturb post-Golgi trafficking of membrane proteins. *Nat Commun* 2013;**4**:1846. https://doi.org/10.1038/ncomms2873.
117 Cohen E, Taraboulos A. Scrapie-like prion protein accumulates in aggresomes of cyclosporin A-treated cells. *EMBO J* 2003;**22**:404–17. https://doi.org/10.1093/emboj/cdg045.
118 Serrano C, Lyahyai J, Bolea R, Varona L, Monleón E, Badiola JJ, *et al.* Distinct spatial activation of intrinsic and extrinsic apoptosis pathways in natural scrapie: association with prion-related lesions. *Vet Res* 2009;**40**:42. https://doi.org/10.1051/vetres/2009024.
119 Ettaiche M, Pichot R, Vincent J-P, Chabry J. In Vivo Cytotoxicity of the Prion Protein Fragment 106–126 *. *J Biol Chem* 2000;**275**:36487–90.

https://doi.org/10.1074/jbc.C000579200.
120 Bounhar Y, Zhang Y, Goodyer CG, LeBlanc A. Prion Protein Protects Human Neurons against Bax-mediated Apoptosis*. *J Biol Chem* 2001;**276**:39145–9. https://doi.org/10.1074/jbc.C100443200.
121 Tuğrul B, Balcan E, Öztel Z, Çöllü F, Gürcü B. Prion protein-dependent regulation of p53-MDM2 crosstalk during endoplasmic reticulum stress and doxorubicin treatments might be essential for cell fate in human breast cancer cell line, MCF-7. *Exp Cell Res* 2023;**429**:113656. https://doi.org/10.1016/j.yexcr.2023.113656.
122 Grell M, Zimmermann G, Hülser D, Pfizenmaier K, Scheurich P. TNF receptors TR60 and TR80 can mediate apoptosis via induction of distinct signal pathways. *J Immunol* 1994;**153**:1963–72.
123 Filippi M, Rovaris M, Comi G. *Neurodegeneration in Multiple Sclerosis*. Springer Science & Business Media; 2008.
124 Wang H, Tian C, Xu Y, Xie W-L, Zhang J, Zhang B-Y, *et al.* Abortive cell cycle events in the brains of scrapie-infected hamsters with remarkable decreases of PLK3/Cdc25C and increases of PLK1/cyclin B1. *Mol Neurobiol* 2013;**48**:655–68. https://doi.org/10.1007/s12035-013-8455-1.
125 van de Weerdt BCM, Medema RH. Polo-like kinases: a team in control of the division. *Cell Cycle* 2006;**5**:853–64. https://doi.org/10.4161/cc.5.8.2692.
126 Toyoshima-Morimoto F, Taniguchi E, Nishida E. Plk1 promotes nuclear translocation of human Cdc25C during prophase. *EMBO Rep* 2002;**3**:341–8. https://doi.org/10.1093/embo-reports/kvf069.
127 Jeong J-K, Park S-Y. Neuroprotective effect of cellular prion protein (PrPC) is related with activation of alpha7 nicotinic acetylcholine receptor (α7nAchR)-mediated autophagy flux. *Oncotarget* 2015;**6**:24660–74. https://doi.org/10.18632/oncotarget.4953.
128 Petrakis S, Irinopoulou T, Panagiotidis CH, Engelstein R, Lindstrom J, Orr-Urtreger A, *et al.* Cellular prion protein co-localizes with nAChR beta4 subunit in brain and gastrointestinal tract. *Eur J Neurosci* 2008;**27**:612–20. https://doi.org/10.1111/j.1460-9568.2008.06037.x.
129 Cardinale A, Nastrucci C, Cesario A, Russo P. Nicotine: specific role in angiogenesis, proliferation and apoptosis. *Crit Rev Toxicol* 2012;**42**:68–89. https://doi.org/10.3109/10408444.2011.623150.
130 Picciotto MR, Zoli M. Neuroprotection via nAChRs: the role of nAChRs in neurodegenerative disorders such as Alzheimer’s and Parkinson's disease. *Front Biosci* 2008;**13**:492–504. https://doi.org/10.2741/2695.
131 Richardson DD, Tol S, Valle-Encinas E, Pleguezuelos C, Bierings R, Geerts D, *et al.* The prion protein inhibits monocytic cell migration by stimulating β1 integrin adhesion and uropod formation. *J Cell Sci* 2015;**128**:3018–29. https://doi.org/10.1242/jcs.165365.
132 de Almeida CJG, Chiarini LB, da Silva JP, E Silva PMR, Martins MA, Linden R. The cellular prion protein modulates phagocytosis and inflammatory response. *J Leukoc Biol* 2005;**77**:238–46. https://doi.org/10.1189/jlb.1103531.
133 Onodera T, Sakudo A, Tsubone H, Itohara S. Review of studies that have used knockout mice to assess normal function of prion protein under immunological or

pathophysiological stress. *Microbiol Immunol* 2014;**58**:361–74. https://doi.org/10.1111/1348-0421.12162.
134 Prodromidou K, Papastefanaki F, Sklaviadis T, Matsas R. Functional cross-talk between the cellular prion protein and the neural cell adhesion molecule is critical for neuronal differentiation of neural stem/precursor cells. *Stem Cells* 2014;**32**:1674–87. https://doi.org/10.1002/stem.1663.
135 Steele AD, Emsley JG, Ozdinler PH, Lindquist S, Macklis JD. Prion protein (PrP^c) positively regulates neural precursor proliferation during developmental and adult mammalian neurogenesis. *Proc Natl Acad Sci U S A* 2006;**103**:3416–21. https://doi.org/10.1073/pnas.0511290103.
136 Schmitt-Ulms G, Legname G, Baldwin MA, Ball HL, Bradon N, Bosque PJ, *et al.* Binding of neural cell adhesion molecules (N-CAMs) to the cellular prion protein. *J Mol Biol* 2001;**314**:1209–25. https://doi.org/10.1006/jmbi.2000.5183.
137 Head MW, Ritchie D, Smith N, McLoughlin V, Nailon W, Samad S, *et al.* Peripheral tissue involvement in sporadic, iatrogenic, and variant Creutzfeldt-Jakob disease: an immunohistochemical, quantitative, and biochemical study. *Am J Pathol* 2004;**164**:143–53. https://doi.org/10.1016/S0002-9440(10)63105-7.
138 Glatzel M, Abela E, Maissen M, Aguzzi A. Extraneural Pathologic Prion Protein in Sporadic Creutzfeldt–Jakob Disease. *N Engl J Med* 2003;**349**:1812–20. https://doi.org/10.1056/NEJMoa030351.
139 Porter DD, Porter HG, Cox NA. Failure to demonstrate a humoral immune response to scrapie infection in mice. *J Immunol* 1973;**111**:1407–10. https://doi.org/10.4049/jimmunol.111.5.1407.
140 Heppner FL, Musahl C, Arrighi I, Klein MA, Rülicke T, Oesch B, *et al.* Prevention of scrapie pathogenesis by transgenic expression of anti-prion protein antibodies. *Science* 2001;**294**:178–82. https://doi.org/10.1126/science.1063093.
141 Bessen RA, Wilham JM, Lowe D, Watschke CP, Shearin H, Martinka S, *et al.* Accelerated shedding of prions following damage to the olfactory epithelium. *J Virol* 2012;**86**:1777–88. https://doi.org/10.1128/JVI.06626-11.
142 Goodbrand IA, Ironside JW, Nicolson D, Bell JE. Prion protein accumulation in the spinal cords of patients with sporadic and growth hormone associated Creutzfeldt-Jakob disease. *Neurosci Lett* 1995;**183**:127–30. https://doi.org/10.1016/0304-3940(94)11131-2.
143 Skinner PJ, Abbassi H, Chesebro B, Race RE, Reilly C, Haase AT. Gene expression alterations in brains of mice infected with three strains of scrapie. *BMC Genomics* 2006;**7**:114. https://doi.org/10.1186/1471-2164-7-114.
144 Lupi O. Prions in dermatology. *J Am Acad Dermatol* 2002;**46**:790–3. https://doi.org/10.1067/mjd.2002.120624.
145 Ye X, Carp RI. Histopathological changes in the pituitary glands of female hamsters infected with the 139H strain of scrapie. *J Comp Pathol* 1996;**114**:291–304. https://doi.org/10.1016/s0021-9975(96)80051-x.
146 Viguié C, Chilliard Y, Gayrard V, Picard-Hagen N, Monget P, Dutour A, *et al.* Alterations of somatotropic function in prion disease in sheep. *J Endocrinol* 2004;**183**:427–35. https://doi.org/10.1677/joe.1.05683.
147 Gayrard V, Picard-Hagen N, Grino M, Sauze N, Grandjean C, Galea J, *et al.* Major

hypercorticism is an endocrine feature of ewes with naturally occurring scrapie. *Endocrinology* 2000;**141**:988–94. https://doi.org/10.1210/endo.141.3.7345.
148 O'Hara E, Herbst A, Kommadath A, Aiken JM, McKenzie D, Goodarzi N, *et al.* Neural transcriptomic signature of chronic wasting disease in white-tailed deer. *BMC Genomics* 2022;**23**:69. https://doi.org/10.1186/s12864-022-08306-0.
149 Sharma D, Masison DC. Single methyl group determines prion propagation and protein degradation activities of yeast heat shock protein (Hsp)-70 chaperones Ssa1p and Ssa2p. *Proc Natl Acad Sci U S A* 2011;**108**:13665–70. https://doi.org/10.1073/pnas.1107421108.
150 Tatzelt J, Voellmy R, Welch WJ. Abnormalities in stress proteins in prion diseases. *Cell Mol Neurobiol* 1998;**18**:721–9. https://doi.org/10.1023/a:1020646321841.
151 Newnam GP, Birchmore JL, Chernoff YO. Destabilization and recovery of a yeast prion after mild heat shock. *J Mol Biol* 2011;**408**:432–48. https://doi.org/10.1016/j.jmb.2011.02.034.
152 Kenward N, Hope J, Landon M, Mayer RJ. Expression of polyubiquitin and heat-shock protein 70 genes increases in the later stages of disease progression in scrapie-infected mouse brain. *J Neurochem* 1994;**62**:1870–7. https://doi.org/10.1046/j.1471-4159.1994.62051870.x.